This is to certify that the

thesis entitled

CHARACTERIZATION OF THE SOL-GEL AND MOCVD
PROCESSES FOR THE DEPOSITION OF ALUMINUM
OXIDE THIN FILMS

presented by

Mark Joseph Waner

has been accepted towards fulfillment
of the requirements for

M.S. degree in Chemistry

Major professor

Date April 7, 1994

CHARACTERIZATION OF THE SOL-GEL AND MOCVD PROCESSES FOR THE DEPOSITION OF ALUMINUM OXIDE THIN FILMS

By

Mark Joseph Waner

A THESIS

Submitted to Michigan State University in partial fulfillment of the requirements for the degree of

MASTER OF SCIENCE

Department of Chemistry

1994

ABSTRACT

CHARACTERIZATION OF THE SOL-GEL AND MOCVD PROCESSES FOR THE DEPOSITION OF ALUMINUM OXIDE THIN FILMS

By

Mark Joseph Waner

In this Study the sol-gel solution chemistry of a valerate modified aluminum alkoxide is characterized with FTIR The hydrolysis and condensation of aluminum divalerate species in solution leads to the formation of a gel which is then spin cast and dip coated to form thin films. The films are characterized with FTIR, XPS and SEM, before and after calcination. The layered valerate films form continuous aluminum oxide films when calcined at 400°C.

The effect of substrate and carrier gas on the deposition of aluminum oxide thin films from aluminum acetylacetonate was examined. Films deposited in air have less carbon contamination than those deposited under nitrogen. When KBr, quartz and SiC were compared, KBr produced the least contaminated films, while SiC showed the largest amount of aluminum deposited.

ACKNOWLEDGEMENTS

I would like to thank Dr. Jeffrey Ledford for his guidance, assistance and ideas. Thanks also goes out to my co-workers: Ed, Greg, Jeff, Kathy, Mike, Paul, Per and Radu. A final thanks to my family who have supported my studies from the beginning.

TABLE OF CONTENTS

Page

TABLE OF CONTENTS

LIST OF TABLES

LIST OF FIGURES

Figure Page

LIST OF FIGURES

Chapter 1

Introduction to the Preparation and Characterization of Metal Oxide Diffusion Barrier Coatings

1.1. Overview of Barrier Coatings for use with Silicon Carbide

Silicon carbide is an important component of many advanced materials. Its high strength, hardness, and 2700°C melting point makes SiC quite useful as a structural material. In addition, SiC has a band gap of 2.2 eV and thus is an ideal candidate for a new generation of high temperature electronics capable of handling large amounts of power at high frequency [1].

In recent years the use of ceramic fibers as a reinforcing material for intermetallic matrix composites has received a great deal of attention. The fiber/matrix interface acts as a route for energy dissipation during crack propagation. Ideally, the interaction between the fiber and the matrix should be strong enough for load transfer from the matrix to the fiber to occur, but weak enough that the interface will fail before catastrophic failure of the composite.

Silicon carbide fibers have been shown to be effective as reinforcements in a variety of ceramic (e.g. Al_2O_3, ZrO_2) and glass matrices [2-5]. Silicon carbide has also received much interest as a reinforcement material for intermetallic composites. The use of silicon carbide for this application is generally found to be quite limited, however, due to the reactivity of the fiber with the matrix. It has been shown that SiC will react with many metals, such as Ti [6,7], Nb [8,9], Al [10-12], Fe [13-15] and Ni [16-20] at typical composite fabrication temperatures (> 600°C).

Depending on the metal involved, metal carbides or metal silicides may form as shown in the following reactions:

$$\mathrm{SiC} + 3\,\mathrm{Ni} \longrightarrow \mathrm{Ni_3Si} + \mathrm{C} \qquad (1)$$

$$\mathrm{SiC} + \mathrm{Ti} \longrightarrow \mathrm{TiC} + \mathrm{Si} \qquad (2)$$

In many cases these reactions can consume the fibers, leaving the brittle metal carbides and silicides which degrade the composite performance [21]. The extent of these reactions may be limited if a diffusion barrier is placed between the SiC fiber and the metal matrix. Some of the more effective barrier coatings in use are the refractory metal oxides. A few examples which have shown some chemical compatibility with both the SiC and metal alloy matrix materials are zirconia, yttria stabilized zirconia and alumina [22-25].

1.2. Sol-Gel Route to Metal Oxide Thin Films

One of the most studied low temperature routes to the production of glass and ceramic materials is the solution sol-gel process. Sol-gel chemistry most often involves the formation of metal oxide polymer networks through the controlled hydrolysis and polycondensation of precursor materials, typically aqueous metal cations or metal alkoxides. Through careful control of network formation one may obtain a wide range of products, from monodispersed colloids to thin films and monoliths. Monoliths produced by sol-gel techniques may be used as optical filters and lenses. One of the major commercial uses of sol-gel derived thin films is in the coating of glass in order to modify its optical properties. Alternating layers of silica and titania have found application as coatings to produce automotive rear view mirrors since the 1950's [26]. This same technology has also been successfully used for the coating of large plate glass windows with a solar reflecting titania layer for use in modern buildings [26]. The techniques of spray or dip coating, or spin casting are often used for the formation of sol-gel derived thin films [26].

Through low temperature sintering processes sol-gel glasses may be converted into amorphous ceramic materials. Crystalline ceramics may be obtained by high temperature processing. The low sintering temperature enables the fabrication of novel glasses and ceramic materials which are not compatible at the high temperatures of conventional ceramic and glass production. In addition to new combinations of glass and ceramic materials, low temperature processing also enables the modification of inorganic networks with organic functional groups. This is currently of interest to the optical chemical sensor field, since inorganic and organic guest molecules can be incorporated into monoliths and thin films of glass and ceramic materials [27-29].

A sol is best described as a suspension or dispersion of colloidal particles (10-1000 Å) in solution. The gel state is not well defined, but can be thought of as an amorphous colloidal solid which has some liquid component dispersed throughout. In practice it is not possible to determine precisely the point at which a sol transforms into a gel or to measure an activation energy for the process. Hench and West define a gel as a material that can support a stress elastically [30]. As the sol becomes a gel, colloidal particles interconnect. Once discrete particles are connected, the newly formed network continues to connect to other particles and networks.

Although many early sol-gel processes involved the use of metal nitrates or halides, the hydrolysis of metal alkoxides has received more attention recently. Besides the ease of hydrolysis, metal alkoxides also have physical and chemical properties which make them appropriate for use as sol-gel precursors. First, synthesis of metal alkoxides is, in general, quite facile. Many alkoxides are synthesized simply by reacting the pure metal with an alcohol [31]:

$$Al \quad + \quad 3C_2H_5OH \xrightarrow{I_2} Al(OC_2H_5)_3 \; + \; \tfrac{3}{2}H_2 \qquad (3)$$

Another widely used synthesis technique is a ligand exchange reaction utilizing the parent alcohol of the desired alkoxide as the solvent [48]:

$$SiCl_4 \; + \; 4C_2H_5OH \longrightarrow Si(OC_2H_5)_4 \; + \; 4HCl \qquad (4)$$

Secondly, most metal alkoxides are easily purified either by distillation or recrystallization [31]. In addition, the metal alkoxides are soluble in a range of organic solvents, most notably in solutions of their parent alcohol. This property is critical to the sol-gel process. Since most sol-gel syntheses involve the hydrolysis of alkoxides, and are often catalyzed by acids or bases, it is important that the alkoxide be soluble in water miscible solvents such as alcohols.

The formation of the inorganic network involves two competing types of reaction: hydrolysis and condensation. The reaction scheme is most simply illustrated as:

$$M(OR)_n \; + \; XOH \longrightarrow M(OR)_{n-x}(OX)_x \; + \; ROH$$

The Lewis acidity of the metal center is the major driving force for this reaction scheme. The reactions occur by a S_N2 nucleophilic substitution reaction illustrated below:

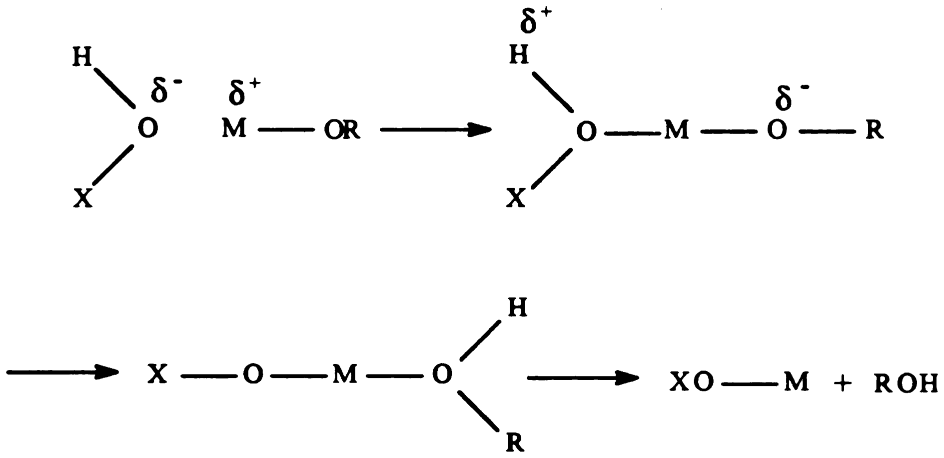

(5)

X represents hydrogen for a hydrolysis reaction or a metal center in the case of a condensation reaction. In some cases a third type of substitution reaction which may occur is a complexation reaction, where X represents some nucleophilic ligand.

The condensation reaction may occur by two different mechanisms, olation and oxolation. The dominant reaction pathway depends both on the degree of hydrolysis and the stability of the various metal species in found in the solution.

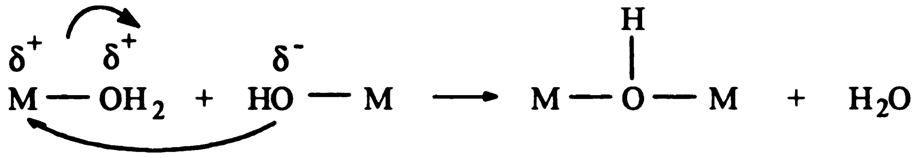

$$\overset{\delta^+}{M} - \overset{\delta^+}{OH_2} + \overset{\delta^-}{HO} - M \longrightarrow M - \overset{\overset{\textstyle H}{|}}{O} - M + H_2O \qquad (6)$$

Oxolation may occur along with olation when aquo precursors are available, and exclusively when only hydroxyl species are available. Oxolation is a two step process: first a nucleophilic addition of the hydroxyl group followed by a 1,3 proton transfer.

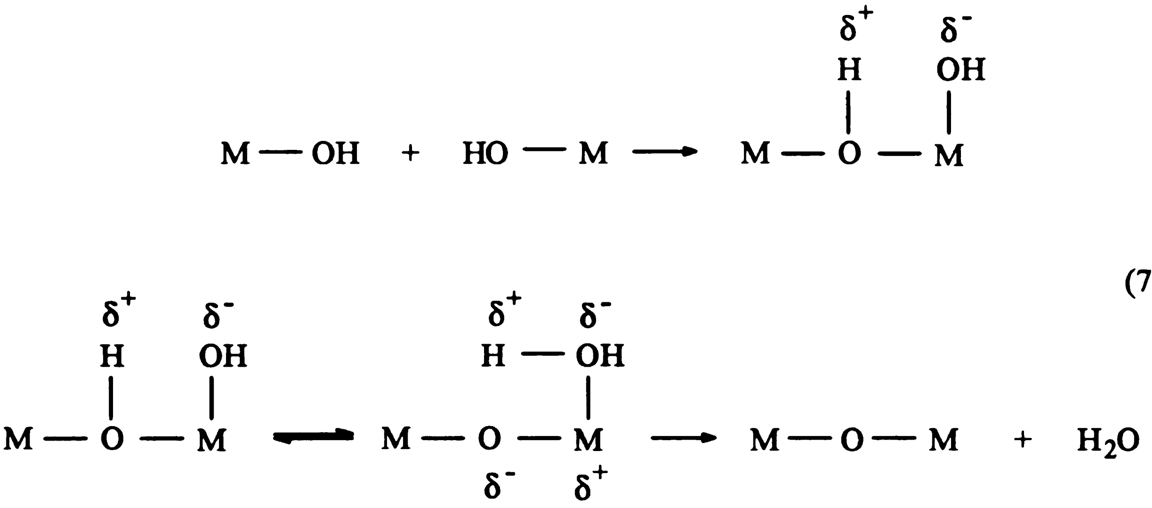

$$\mathrm{M{-}OH} + \mathrm{HO{-}M} \longrightarrow \mathrm{M}{-}\overset{\overset{\delta^+}{\mathrm{H}}}{\mathrm{O}}{-}\overset{\overset{\delta^-}{\mathrm{OH}}}{\mathrm{M}}$$

(7)

$$\mathrm{M}{-}\overset{\overset{\delta^+}{\mathrm{H}}}{\mathrm{O}}{-}\overset{\overset{\delta^-}{\mathrm{OH}}}{\mathrm{M}} \longrightarrow \mathrm{M}{-}\underset{\delta^-}{\overset{\overset{\delta^+}{\mathrm{H}}{-}}{\mathrm{O}}}{-}\underset{\delta^+}{\overset{\overset{\delta^-}{\mathrm{OH}}}{\mathrm{M}}} \longrightarrow \mathrm{M{-}O{-}M} + H_2O$$

The reactivity of the alkoxide has a great deal to do both with the nature of the metal center and the alkoxy group used. The reactivity of an alkoxide will increase with the size and inversely with the electronegativity of the metal center [31,32]. Thus alkoxide reactivity should increase as one goes down a group in the periodic table. The alkoxy ligand can also have a dramatic effect on the hydrolysis and condensation reactions [31,32]. The inductive effect of the alkyl group influences the effective electropositivity of the metal center. In addition the size and the steric bulk of the alkoxy group can be modified in order to control the reactivity of a metal center [31].

While the mechanistic details of silicon sol-gel chemistry are well established [33-37], the understanding of other main group and transition metal sol-gel chemistry is quite limited. Further, whereas silicon alkoxides hydrolyze slowly and gel formation is quite slow, the rate of hydrolysis for transition metal alkoxides is many orders of magnitude faster. The two major factors which account for this difference are that most transition metals can have multiple coordinations and, compared to silicon, they are much more electropositive [31]. When multiple coordination numbers are possible, a transition metal complex with a low coordination number may undergo nucleophilic attack through a coordination expansion. The higher electropositivity of the transition metals makes them more susceptible to nucleophilic attack.

In general, when dealing with sol-gel processes involving silicon alkoxides the reaction rate must be increased in order to obtain a gel with desired physical properties (i.e. particle size, pore volume, etc.). This is usually achieved through the use of acid or base catalysts and small alkoxy ligands such as ethoxide and methoxide. In the case of transition metal sol-gel synthesis, the hydrolysis and condensation reactions often must be slowed down in order to obtain a gel, rather than a precipitate. This control is most often achieved through the use of complexing ligands bound to the metal center. A complexing ligand can lower the reactivity of the metal by decreasing the electropositivity of the metal and/or by steric hindrance. The reagents most often used are organic acids and β-diketones [38-47]. Organic acids are more strongly binding ligands than the alkoxides and therefore, make the metal center more stable with respect to hydrolysis. The role of organic acids in the control of titanium and zirconium alkoxide hydrolysis has received some attention in the literature [41-43,47-51]. β-diketones are strongly binding chelating ligands which can decrease the rate of nucleophilic attack at the metal center due to the chelation effect and steric hindrance.

The hydrolysis of aluminum ions has been investigated for over a century [52]. The classical studies of aluminum sol-gel chemistry involve the hydrolysis of aqueous aluminum ions. In the 1970's Yoldas found that large monoliths of aluminum oxide could be produced through the hydrolysis and polycondensation of aluminum alkoxides [53,54]. Although differing in synthesis, the products obtained by the hydrolysis of aqueous solutions are quite similar to the products obtained by the Yoldas method. Brinker and Scherer note that this similarity may have much to do with the large excess of water in each of the synthesis methods [52]. The study of aluminum sol-gel chemistry in solutions of low water concentration has received very little attention in the literature [52].

The typical sol-gel synthesis involves the hydrolysis of a metal alkoxide in an excess of water (i.e. ~100:1 water : alkoxide molar ratio). In some cases small amounts of acid or base are used as a catalyst for the hydrolysis and/or condensation reaction, typically the acid or base to alkoxide ratio is ≤ 1. The conditions for synthesis are highly dependent on the nature of the alkoxide used. Recently, however, Berglund *et al.* [48,51] have shown that high quality films may be produced using a large excess of organic acids with titanium and zirconium propoxide systems. In these syntheses low molar ratios of water to alkoxide were used (i.e. ~1.5). One of these studies carefully examined the effect of carboxyl chain length and acid to alkoxide molar ratio on the film quality [48]. For titanium isopropoxide sol-gel it was observed that the best films were obtained when the relatively long chain (valeric and butyric) acids were used, while shorter (propionic) and longer (hexanoic) carboxylic acids gave fairly poor quality films [48]. It was proposed that the shorter chains don't provide sufficient steric or nucleophilic hindrance, while the very long chain acids hinder the polymerization reactions [48].

1.3. Metal Organic Chemical Vapor Deposition (MOCVD)

Chemical vapor deposition (CVD) techniques have been in use for many years as a synthetic route to refractory compounds at reduced temperatures [61]. A typical CVD process involves the reaction of gas phase molecules at a hot substrate surface. A wide variety of reaction types have been utilized, such as pyrolysis, oxidation-reduction, and hydrolysis [55]. The use of reactive pathways to film deposition separates CVD from the physical vapor deposition (PVD) techniques such as evaporation and sputter coating. The classical CVD processes typically involve the reactions of metal halides or hydrides as precursors, and require temperatures in excess of 1000°C. More recently metal-organic chemical vapor deposition (MOCVD) techniques have been widely studied as pathways to coatings at even lower temperatures. An example of the utility of organometallic precursors involves the deposition of silicon nitride. The classical CVD process for deposition of silicon nitride is given by

$$SiH_4 + NH_3 \xrightarrow{>1000°C} Si_3N_4 \qquad (8)$$

while Fix *et al.* [56] have reported deposition of silicon nitride at temperatures as low as 600°C

$$H_xSi(N(CH_3)_2)_{4-x} \xrightarrow{600°C} Si_3N_4 \qquad (9)$$

There are five basic steps in the general CVD mechanism (Figure 1.1), any of which may be the rate determining step for a particular deposition [55]. Once the reactant species are in the gas phase, usually diluted by a carrier gas stream, they must diffuse to the substrate surface. Reactant gases that have diffused through the boundary layer must be adsorbed onto the substrate. The adsorption process is followed by surface chemical interactions which lead directly to the deposition products. Besides various types of reactions, surface interactions may also involve lattice incorporation or surface diffusion [55]. Once the solid reaction products have formed on the substrate, the byproducts of the reaction, which by design should be volatile species, desorb from the surface. The final step in this general mechanism is the diffusion of the byproducts from the surface region into the carrier gas stream. The kinetics of these processes will often determine many of the film characteristics and properties [57,58].

MOCVD processing has become a popular coating technique because of the low temperatures generally involved in the volatilization and decomposition of metal-organic precursors. However, it is the ability to tailor the properties of precursors that has attracted the interest of most chemists. In these methods organo-metallic compounds are designed to provide a core composition around the metal center which is similar in both stoichiometry and structure to the desired coating. Ligands are chosen to enhance the volatility of the precursor and reduce gas phase oligomerization. Figure 1.2 shows an

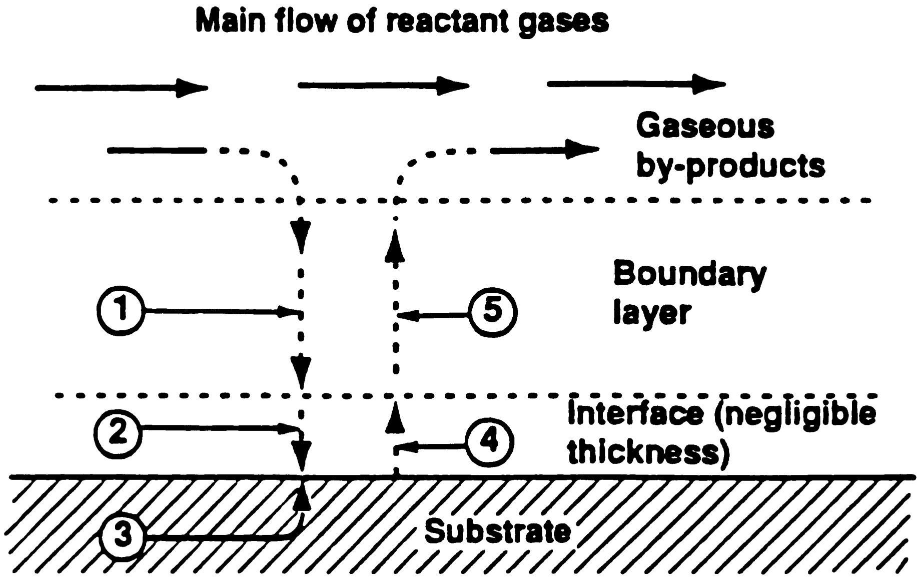

1. Diffusion in of reactants through boundary layer
2. Adsorption of reactants on substrate
3. Chemical reaction takes place
4. Desorption of adsorbed species
5. Diffusion out of by-products

Figure 1.1: CVD Mechanism [55]

interesting example of this approach, studied by Interrante *et al.* [59], which involves the use of $[(CH_3)_2AlNH_2]_3$ as a precursor to aluminum nitride.

The preparation of useful coatings (i.e., desired stoichiometry and morphology) using MOCVD relies on the interaction of many complex factors. The partial pressures of carrier and reactant gases, temperature gradients, fluid flow dynamics of the system and the composition of the precursor and substrate all influence the structure and composition of the final product [61,60]. The mean free path of the vapor phase reactants and the diffusion properties of the substrate surface will play a major role in the coating morphology [58]. Fischer *et al.* [61] noted that for deposition involving the pyrolysis of an organometallic compound such as alkoxides and β-diketonates, the use of a carrier gas with an oxygen source tends to limit carbon contamination in the deposited films. Although the effect of various precursors, carrier gases and temperatures for many CVD processes have been studied, relatively little attention has been given to the effect of the substrate composition and structure.

There has been much investigation of oxide coating deposition by CVD processes [55,62]. Since the discovery of the high T_c Y-Ba-Cu oxide superconductors, however, the MOCVD technique has become the focus of increased effort for the deposition of oxide coatings [63-65]. Larkin *et al.* [59] have used the MOCVD process to deposit thin barrier coatings of yttria onto a silicon carbide fiber at 630°C using yttrium β-diketonate precursors Although this was found to be an effective coating for preventing interfacial reactions, the coatings produced were not continuous. Additionally, in many CVD processes problems arise due to the co-deposition of carbon and slow growth rates of films. While high quality and high purity coatings are commercially produced in electronics applications, the equipment and materials used are costly. Through a better understanding of the effect of all CVD parameters, the use of CVD techniques can be improved.

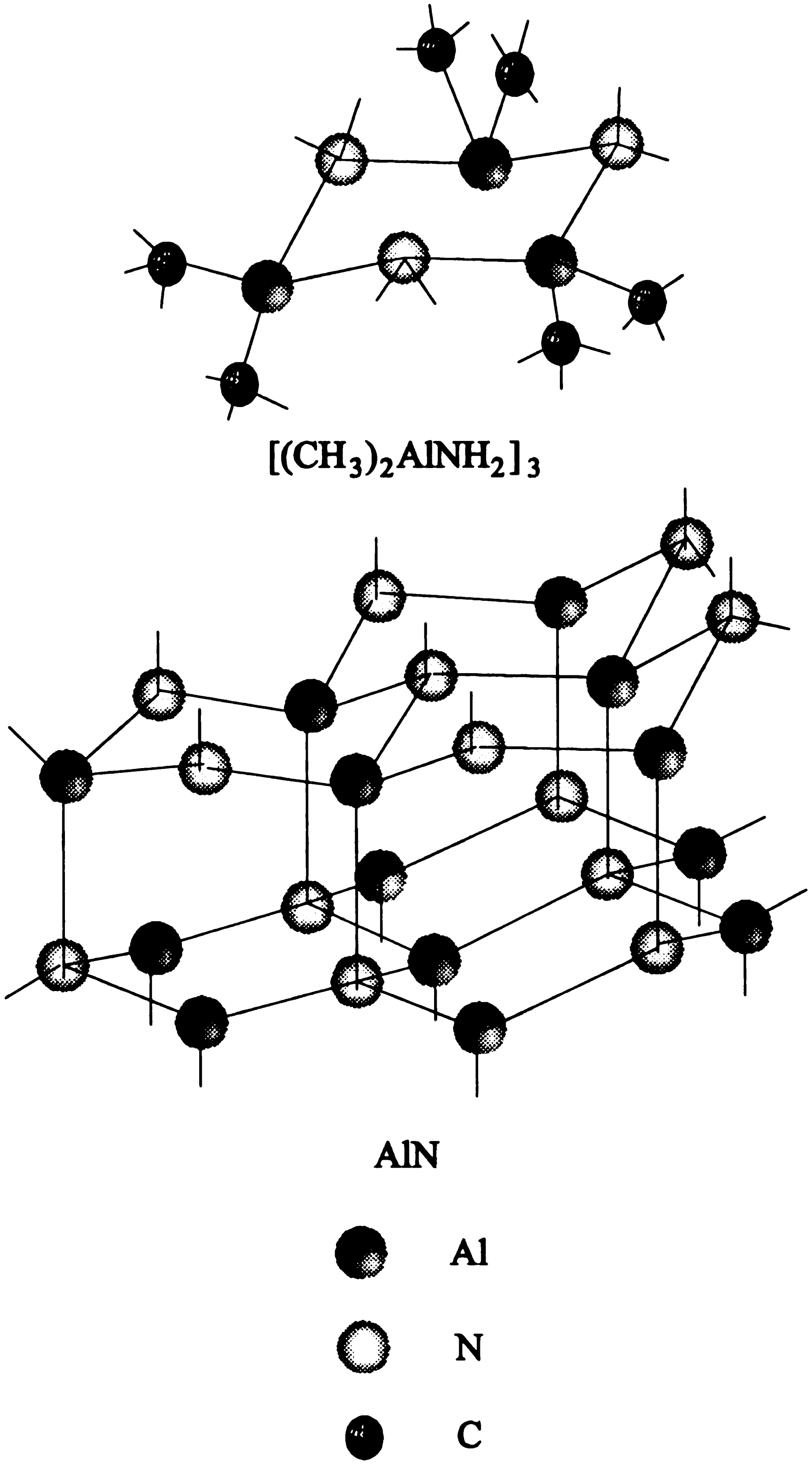

Figure 1.2 : Example of Precursor Design in MOCVD

1.4. Materials Characterization

In order to understand the sol-gel and MOCVD processes we need to obtain detailed molecular level information. For the MOCVD process we need to understand better the chemical processes which occur at the surface of the substrate. In the sol-gel process we would like to understand the reaction process which leads to the thin film formation and to characterize the structure of the oxide films produced. Fourier transform infrared spectroscopy (FTIR) will provide information which describes the molecular level structures involved in sol-gel syntheses and the films produced. X-ray photoelectron spectroscopy (XPS) will be used to provide both structural information as well as stoichiometric information relevant to the films produced. We will also be using scanning electron microscopy (SEM) in order to examine the surface morphology of the coatings and substrates used.

X-ray Photoelectron Spectroscopy (XPS)

In XPS an X-ray photon transfers its kinetic energy to an atom, causing the ejection of an electron by the photoelectric effect. Conservation of energy requires that

$$h\nu + E^{i}_{tot} = E_{kin} + E^{f}_{tot} \qquad (10)$$

where E^{i}_{tot} and E^{f}_{tot} are the total energies of the initial and final states, respectively, and E_{kin} is the kinetic energy of the photoelectron produced. The binding energy of the electron, referenced to the vacuum level is then equal to

$$E^{v}_{B} = E^{f}_{tot} - E^{i}_{tot} \qquad (11)$$

When (10) and (11) are combined they yield the photoelectric equation

$$h\nu = E_{kin} + E_B^V \qquad (12)$$

When measuring the binding energy of a solid sample the energy scale is referenced to the Fermi level. When a metal sample is examined, an electrical contact is made between the sample and the spectrometer. Since the sample and spectrometer are now in thermodynamic equilibrium, they have the same Fermi level. However, the vacuum level may be different for the sample and the spectrometer. The work function, Φ is used to describe the difference between the Fermi level and the vacuum level. Photoelectrons feel a potential which is equal to the difference between the spectrometer and sample work functions, which leads to the measured kinetic energy being lower than the kinetic energy of the ejected electron.

$$E_{kin}^{meas} = E_{kin} - (\phi_{spec} - \phi_{sample}) \quad (13)$$

The binding energy, referenced to the Fermi level may then be written as

$$E_B^F = h\nu - (E_{kin}^{meas} + \phi_{spec}) \qquad (14)$$

The relationship between these energy levels for XPS of a metal sample is illustrated in Figure 1.3 [66].

Magnesium and aluminum K_α (1253.6 eV and 1486.6 eV respectively) are the most commonly used X-ray lines for XPS. These X-rays are of high enough energy to generate photoelectrons from the core levels, as well as valence shells.

In the analysis of solids, low intensity peaks are observed at higher binding energy than the photoelectron signals. These features are due to the energy loss which occurs when a photoelectron excites a plasmon oscillation in the sample. A classical model is often used to predict the plasmon frequency. In the model a solid is pictured as a collection of positively charged spheres within a sea of electrons. If the electron gas expands δr from its equilibrium radius, where n is the number of electrons in the shell, an electric field, ξ, will be produced.

$$\xi = \frac{q}{r^2} \cdot \delta n = 4\pi n q \, \delta r \qquad (15)$$

Where q is the charge on an electron. The force generated by this field is given by

$$F = -q\xi = -4\pi \, q^2 n \delta \, r \quad (16)$$

Using the harmonic oscillator approximation the frequency of the plasmon vibration is given by

$$\omega_p = \left(\frac{4\pi \, q^2 n}{m} \right)^{1/2} \qquad (17)$$

While the interaction region of X-ray photons with solids is on the order of micrometers, the discrete peaks observed are attributed to electrons which escape from the top 20-50 Å of the sample. The electrons produced deeper in the solid contribute to the backround observed in XPS. Each inelastic interaction which an electron undergoes will lower its kinetic energy and alter its trajectory. The surface sensitivity of electron spectroscopies, such as XPS, derives from the limited mean free path of electrons within a solid. The plot shown in Figure 1.4 is the mean free path of electrons versus the electron kinetic energy [69]. At kinetic energies below the plasmon energy, the most likely scattering processes involve discrete excitation of the valence electrons. At higher kinetic

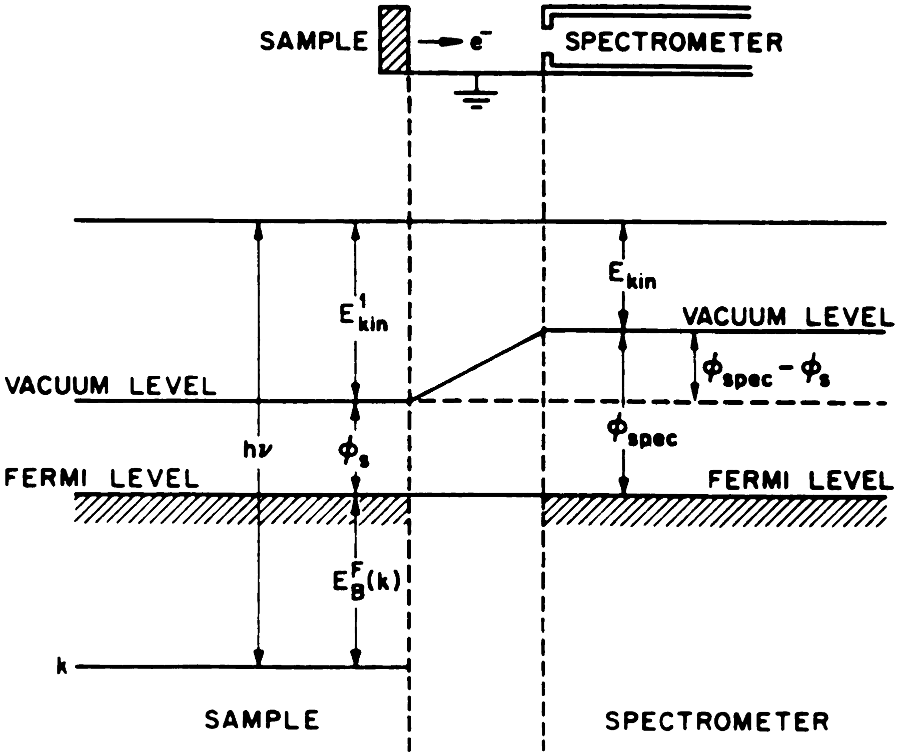

Figure 1.3: XPS Energy Level Diagram [66]

energies the most common inelastic collisions involving photoelectrons are plasmon excitations. When excitation of the plasmon frequency is the dominant source of photoelectron energy loss, the mean free path, λ, may be written as

$$\frac{1}{\lambda}=\left(\frac{\omega_p e^2}{\hbar v^2}\right)\ln\frac{2mv^2}{\hbar\omega_p} \qquad (18)$$

Where v is the velocity of the electron and e is the charge on the electron. The escape depth, 3λ, is then on the order of 15-150Å for most samples.

Besides being able to determine the identity of the atoms in the surface region of a solid, the binding energy of photoelectrons can be used to determine atoms which are in different chemical environments. A binding energy shift, which is often called a chemical shift, is observed for atoms which are in different oxidation states, or in different lattice sites or bonding environments. The binding energy shift has as its physical basis that electrons which are subjected to different potentials will have different energies. As a first approximation the charge potential model proves to be effective for predicting the observed binding energy shift for many systems. This model assumes a hollow sphere of radius r, whose surface has a charge q, equal to the charge of the valence electron shell.

$$E_i = E_i^0 + kq_i + \sum \frac{q_j}{r_{ij}} \qquad (19)$$

where E_i is the binding energy of a core level electron on atom i, $E^0{}_i$ is an energy reference and q_i is the charge on atom i. The final term is a summation of the potential at atom i due to the surrounding atoms, j, which are treated as point charges. From this purely Coulombic treatment the chemical shift for the initial state comes from the displacement of electrostatic potential, as in the case of an electronegative ligand drawing

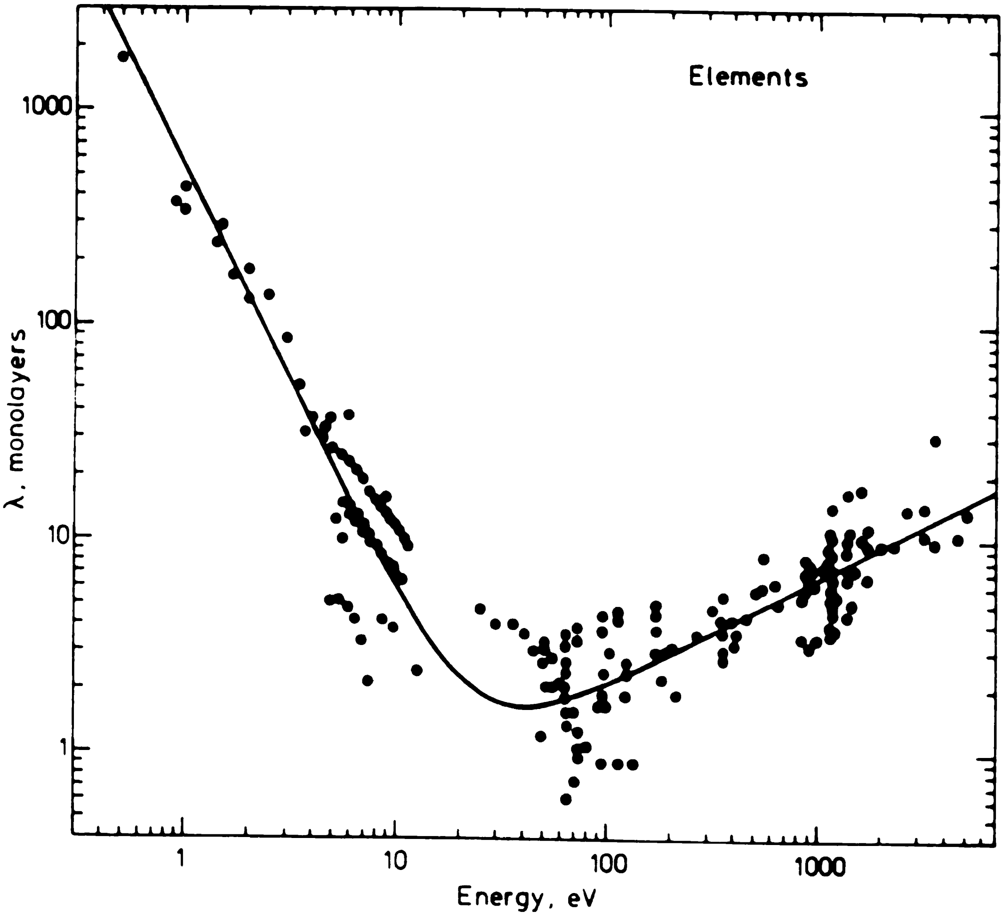

Figure 1.4: Inelastic Mean Free Path for Low Energy Electrons [69]

electron density away from a metal center. There is also a shift for the final state due to the polarization which the atom feels due to the creation of a hole. The core level binding energy shift for atom i in two chemically different environments is given by

$$\Delta E_i = k\,\Delta q + \Delta V_i \qquad (20)$$

where V_i is given by

$$V_i = \sum_{i \neq j} \frac{q_i}{r_{ij}} \qquad (21)$$

This is strictly true only when the work function is the same for each material, which is true for conductors, but not insulators. This model predicts that the chemical shift for all the core levels, assuming no core-valence interaction, is the same since each level is within the same sphere of potential. This model also predicts that as the radius r_{ij} increases the binding energy shift for the same change in electron density will be lower. Although a simple model, it is quite useful for predicting experimentally observed phenomena. Ethyl trifluoroacetate is a good example of the chemical shift effect. This compound has four carbon atoms which are all chemically different. It is seen from Figure 1.5 that the binding energy shifts observed for each type of carbon can be easily resolved by an electron spectrometer [66]. The binding energy shift effect will be used in this thesis to examine the differences between different chemical environments of carbon, oxygen and silicon.

In addition to providing information on chemical identity and environment, XPS is also a useful tool for quantitative analysis of surface stoichiometry. The energy analyzers used in XPS are generally operated in a pulse counting mode, so that the spectra are presented as the number of photoelectrons counted as a function of energy. The number of atoms of a given element can be written as a function of the measured intensity.

$$n = \frac{I}{\sigma \lambda D} \qquad (22)$$

where I is the intensity, σ is the photoionization cross section, λ is the electron mean free path, D is the analyzer detection efficiency. Scofield has calculated the photoionization cross sections, σ, for both Mg and Al Kα radiation, treating the electrons of the final and initial states as moving in the same Hartree-Slater potential [67]. Both theoretical [68] and experimental [69] determinations of the mean free path, λ, for various materials have been made. The detection efficiency is a function of operating mode of the spectrometer and usually varies inversely with kinetic energy. Due to uncertainties in the, λ, σ and D the error associated with absolute quantitation is around ±30% for XPS [70]. However, the quantitation of atomic ratios can be calculated by

$$\frac{n_A}{n_B} = \frac{I_A \sigma_B \lambda_B D_B}{I_B \sigma_A \lambda_A D_A} \qquad (23)$$

In practice the photoionization cross section, mean free path and detection efficiency can be grouped together into one term and called a sensitivity factor. When empirically derived sensitivity factors, such as those found in Appendix 5 of *Practical Surface Analysis by Auger and X-ray Photoelectron Spectroscopy* [69] are used to calculate relative atomic ratios the error can be ±5% [70].

One limitation of the XPS technique, as it relates to the current study, is that it cannot differentiate between very thin continuous films (i.e. ≤ 50 Å) and thicker but discontinuous films. Since the photoelectrons have an escape depth on the order of 100 Å or less, silicon 2p photoelectrons from the silicon carbide substrate would be detected in both very thin continuous films and also in discontinuous films of 100 Å or more. This phenomenon is illustrated in Figure 1.6.

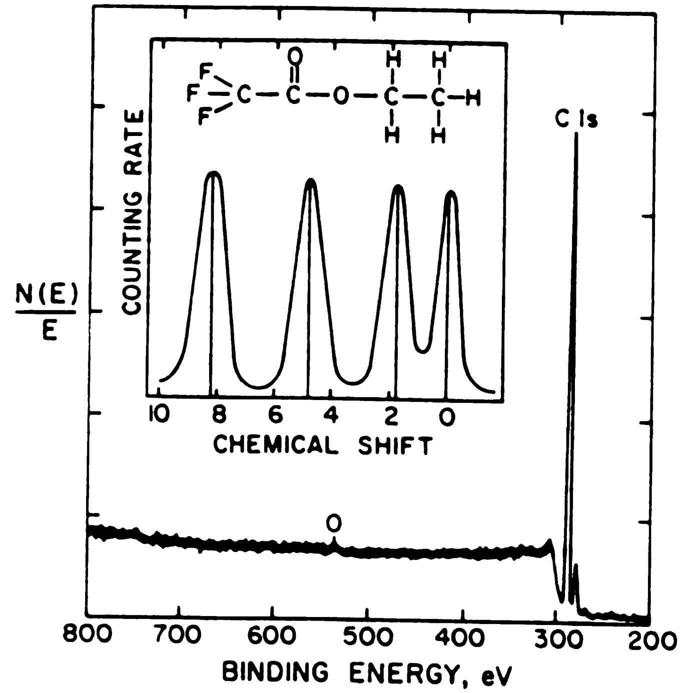

Figure 1.5: XPS Chemical Shift Effect [66]

Scanning Electron Microscopy (SEM)

Scanning electron microscopy makes use of the interaction of a rastered electron beam with a solid surface. A schematic diagram of a basic SEM is shown in Figure 1.7. Electrostatic lenses allow a beam of electrons to be focused down to a spot size of 5-200 nm at the sample surface. The most common SEM technique involves the measurement of the inelastically scattered secondary electrons. Secondary electrons are produced due to the collision of a beam electron with a conduction electron in the sample. Because of the low angle scattering of secondary electrons, the beam which exits the sample is not much wider than the incoming beam. The limit for the image resolution is then dependent more on the spot size of the incoming beam. The secondary electron image is primarily dependent on the surface morphology, since more secondary electrons will be produced from a protrusion in the surface than from a pore as shown in Figure 1.8 [71].

The secondary electrons are typically detected with an Everhart-Thornley detector, which uses a scintillator connected to a photomultiplier tube. Although secondary electrons are emitted in all directions, because of their low kinetic energy (3-5 eV), they can be deflected toward the detector by application of a small potential field. This is useful since the sample/beam interactions also produce elastically backscattered electrons. Backscattered electrons have a kinetic energy on the order of 1-100 keV, and are thus not easily deflected by a small potential field. Therefore, only the backscattered electrons which are emitted in the direction of the detector will be detected with the secondary electrons. Although the high energy primary electron beam has a relatively large depth of interaction in the sample, the mean free path for the low energy secondary electrons limits the depth of detection to about 50 Å for metals and 500 Å for insulators.

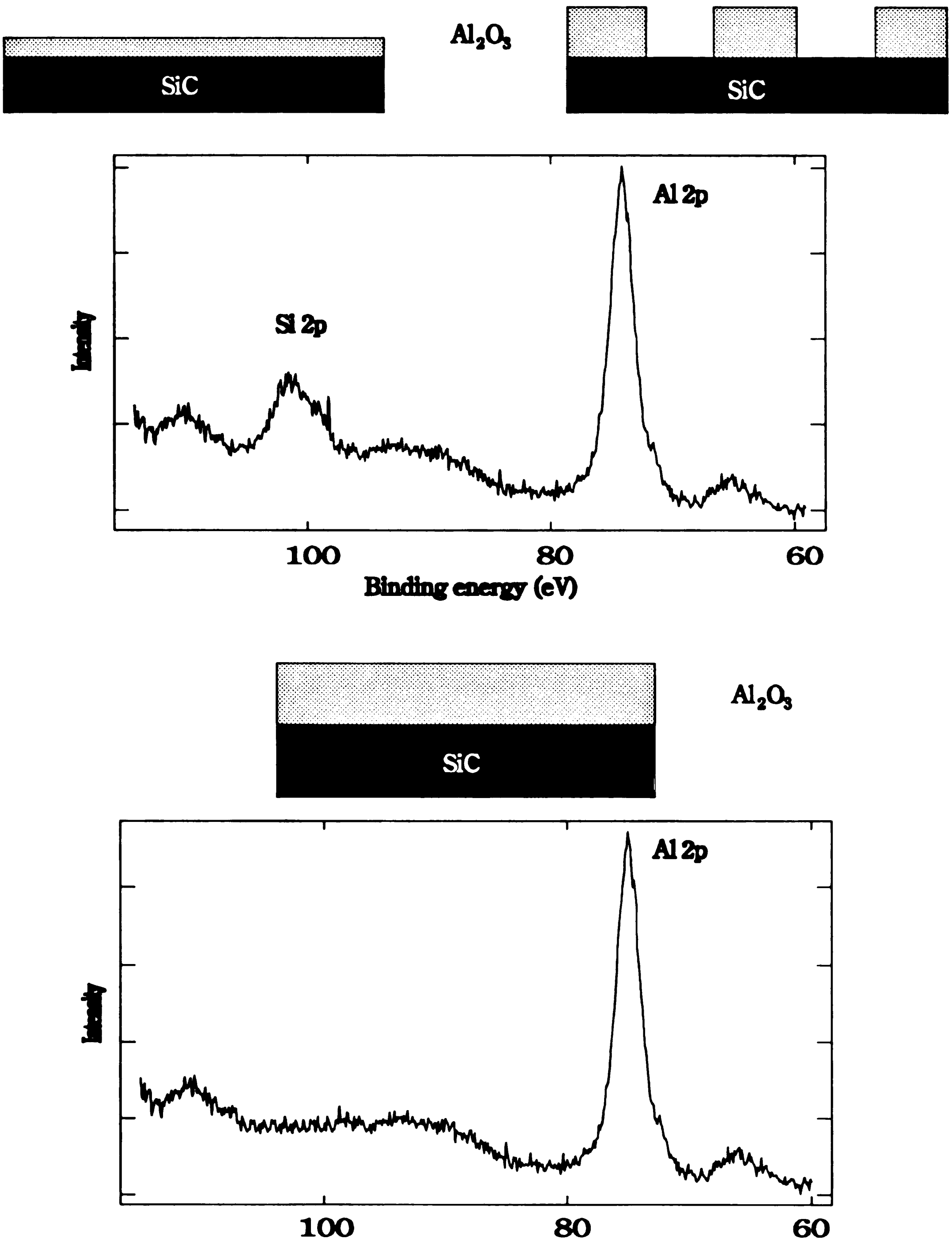

Figure 1.6: Limitation of XPS for Thin Film Analysis

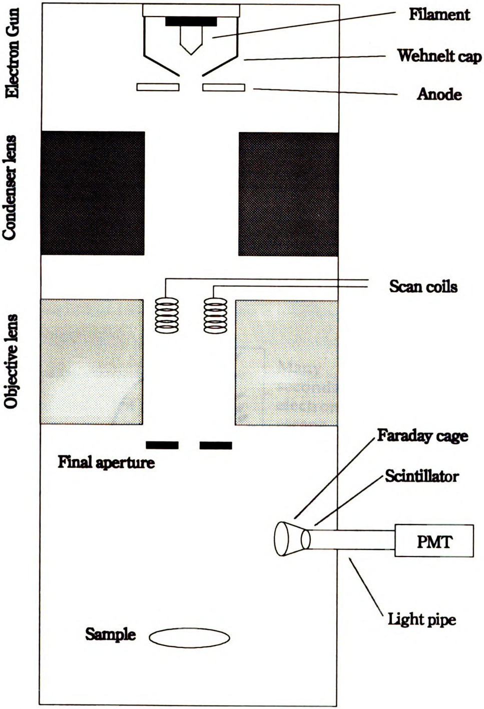

Figure 1.7: SEM Schematic

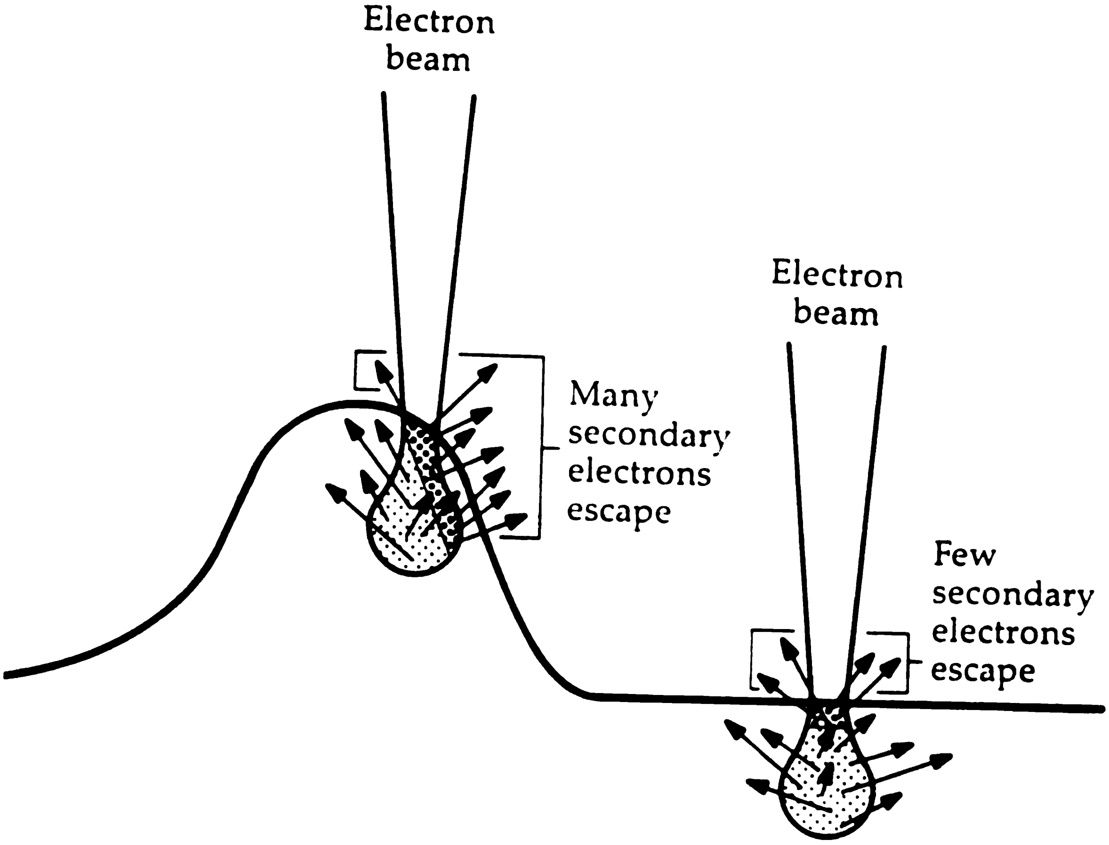

Figure 1.8: SEM-Surface Morphology [71]

1.5. Focus of Research

Sol-Gel Synthesis of Aluminum Oxide Thin Films

The present work will first focus on the formation of aluminum oxide thin films through a new sol-gel synthesis using aluminum isopropoxide, which is first modified using valeric acid and then hydrolyzed in an isopropanol solvent. As this is a new synthesis procedure we would not only like to characterize the structure of the films produced, but also to examine the structure of the intermediates in the reaction sequence. Fourier transform infrared spectroscopy (FTIR) will be used to determine the structure and types of ligand binding in the reaction solutions, as well as of the as cast and calcined films. XPS will be used as a tool for determination of stoichiometry and the oxidation states of the aluminum, carbon and oxygen atoms in the surface region of the as cast and calcined films. SEM analysis will allow us to characterize the surface morphology of the films deposited. Using all of this information we will present a chemical picture of the aluminum sol-gel process.

MOCVD of Aluminum Oxide Coatings

The role of many parameters in CVD processes have been examined in the literature. One role which has not been given much mention is the effect of the substrate composition on the deposition of thin films. The purpose of this work is to examine the role which substrate structure plays in the MOCVD process. SEM analyses will give information about the surface morphology of the silicon carbide, quartz and potassium bromide substrates. Thin films, based on the pyrolysis of aluminum acetylacetonate, will be deposited onto each substrate. FTIR will be used to characterize the structure of the films deposited onto the KBr. XPS will be used to probe the composition and structure of the deposited films. We will use these data to determine what effect, if any, the substrate has on the pyrolysis process.

References

1. *Mat. Res. Soc. Symp. Proc.* 242, Moustakas, T.D.; Pankove, J.I.; Hamakawa, Y., Eds.; Materials Research Society, Pittsburgh, 1992.
2. Becher, P.F.; Wei, G.C. *J. Am. Ceram. Soc.*, **1984,** 67(12), C267.
3. Samanta, S.C.; Musikant, S. *Ceram. Eng. and Sci. Proc.*, **1985,** 6(7-8), 663.
4. Panda, P.C.; Seydel, E.R. *Am. Ceram. Soc. Bull.*, **1985**, 65(2), 338.
5. Gadkaree, K.P.; Chyung, K. *Am. Ceram. Soc. Bull.*, **1986**, 65(2), 370.
6. Bellina, J.J., Jr.; Zeller, M.V. in *Mat. Res. Soc. Symp. Proc.* 97, Materials Research Society, Pittsburgh, 1987, 265.
7. Hasegawa, S.; Nakamura , S.; Kawamoto, N.; Kishibe, H.; Mizokawa, Y. *Surf. Sci.*, **1988**, 206, L851.
8. Yaney, D.L.; Joshi, A. *J. Mater. Res.*, **1990**, 5(10), 2197.
9. Misra, A.K. *J. Mater. Res.*, **1990**, 5(7), 1561.
10. Draper, S.L.; Gaydosh, D.J.; Nathal, M.V.; Misra, A.K. *J. Mater. Res.*, **1990,** 5(9), 1976.
11. Foister, S.A.M.; Johnston, M.W.; Little, J.A. *J. Mat. Sci. Lett.*, **1993,** 12, 209.
12. Shinoda, T.; Liu, H.; Mishima, Y.; Suzuki, T. *Mat. Sci. Eng.*, **1991**, A146, 91.
13. Kaplan, R.; Klein, P.H.; Addamiano, A. *J. Appl. Phys.*, **1985,** 58(1), 321.
14. Mizokawa, Y.; Nakanishi, S.; Miyase, S. *Jpn. J. Appl. Phys.*, 1989, 28(12), 2570.
15. Mizokawa, Y.; Nakanishi, S.; Miyase, S. *Jpn. J. Appl. Phys.*, 1989, 28(12), 2576.
16. Addhoum, H.; Broussaud, D. *Mat. Sci. Eng.*, **1989**, A109, 379.
17. Chouand, T.C.; Nieh, T.G. *J. Mater. Res.*, **1990**, 5(9), 1985.
18. Eustathopoulos, N.; Chatain, D.; Coudurier, L.; *Mat. Sci. Eng.*, **1991**, A135, 83.
19. Nikolopoulos, P.; Agathopoulos, S.; Angelopoulos, G.N.; Naoumidis, A.; Grubmeirer, H. *J. Mat. Sci.*,**1992**, 27, 139.
20. Yang, J.M.; Kao, W.H.; Liu, C.T. *Metall. Trans. A*, **1989**, 20A, 2459.
21. Larkin, D.J.; Interrante, L.V.; Bose, A. *J. Mater. Res.*, **1990**, 5(11), 2706.
22. Misra, A.K. *Metall. Trans A*, 1990, 21A, 441. **1990**
23. Bilba, K.; Manaud, J.P.; Le Petitcorps, Y.; Quenisset, J.M. *Mat. Sci. Eng.*, **1991**, A135, 141.
24. Kieschke, R.R.; Clyne, T.W. *Mat. Sci. Eng.*, **1991**, A135, 145.
25. Misra, A.K. *J. Mater. Res.*, **1990**, 5(7), 1561.
26. Dislich, H. in *Sol-Gel Technology for Thin Films, Fibers, Preforms, Electronics, and Specialty Shapes*, Klein, L.C.,Ed.; Noyes Publications, Park Ridge, NJ: 1988, 50
27. Avnir, D.; Levy, D.; Reisfeld, R. *J. Phys. Chem.*, **1984**, 88, 5956.
28. Lessard, R.B.; Wallace, M.M.; Oertling, W.A.; Chang, C.K.; Berglund, Nocera, D.G.; *Mat. Res. Soc. Symp. Proc.*, **1989**, 155, 109.
29. Dulebohn, J.I.; Haefner, S.C.; Berglund, K.A.; Dunbar, K.R. *Chem. Mater.*, **1992,** 4(3), 506.
30. Hench, L.L; West, J.K. *Chem. Rev.*, **1990**, 90, 33.
31. Bradley, D.C.; Mehrotra, R.C.; Gaur, D.P. *Metal Alkoxides;* Academic Press, London, 1978.

32. Livage, J.; Henry, M.; Sanchez, C. *Prog. Solid St. Chem.*, **1988**, 18, 259.
33. Brinker, C.J.; Clark, D.E.; Ulrich, D.R., Eds.; Mat. Res. Soc. Symp. Proc. 32, Materials Research Society, Pittsburgh, 1984.
34. Brinker, C.J.; Clark, D.E.; Ulrich, D.R., Eds.; Mat. Res. Soc. Symp. Proc. 73, Materials Research Society, Pittsburgh, 1986.
35. Brinker, C.J.; Clark, D.E.; Ulrich, D.R., Eds.; Mat. Res. Soc. Symp. Proc. 121, Materials Research Society, Pittsburgh, 1988.
36. Zelinski, B.J.J.; Brinker, C.J.; Clark, D.E.; Ulrich, D.R.,Eds.; Mat. Res. Soc. Symp. Proc. 180, Materials Research Society, Pittsburgh, 1990.
37. Hampden-Smith, M.J.; Klemperer,W.G.; Brinker,C.J., Eds.; Mat. Res. Soc. Symp. Proc. 271, Materials Research Society, Pittsburgh, 1992.
38. Mehrotra, R.C.; Gaur, D.P.; Bohra, R. *Metal β-diketonates and Allied Derivatives*, Academic Press, London, 1978.
39. Mehrotra, R.C.; Bohra, R. *Metal Carboxylates*, Academic Press, London, 1983.
40. Sanchez, C.; Livage, J.; Henry, M.; Babonneau, F. *J. Non-Cryst. Solids*, **1988**, 100, 65.
41. Doeuff, S.; Henry, M.; Sanchez, C.; Livage, J. *J. Non-Cryst. Solids*, **1987**, 89, 206.
42. Atik, M.; Aegerter, M.A. *J. Non-Cryst. Solids*, **1992**, 147&148, 813.
43. Chaumont, D.; Craievich, A.; Zarzycki, J. *J. Non-Cryst. Solids*, **1992**, 147&148, 127.
44. Debsikar, J.C. *J. Non-Cryst. Solids*, **1986**, 87, 343.
45. Kundu, D.; Ganguli, D. *J. Mat. Sci. Lett.*, **1986**, 5, 293.
46. Doeuff, S.; Henry, M.; Sanchez, C.; Livage, J. *J. Non-Cryst. Solids*, **1987**, 89, 84.
47. Leaustic, A.; Riman, R.E. *J. Non-Cryst. Solids*, **1991**, 135, 259.
48. Gagliardi, C.D.; Dunuwila, D.; Berglund, K.A. in Mat. Res. Soc. Symp. Proc. 180; Zelinski, B.J.J.; Brinker, C.J.; Clark, D.E.; Ulrich, D.R.,Eds.; Materials Research Society, Pittsburgh, 1990, 801.
49. Gagliardi, C.D.; Dunuwila, D.; Van Vlierberge-Torgerson, B.A.; Berglund, K.A. in Mat. Res. Soc. Symp. Proc. 271, Hampden-Smith, M.J.; Klemperer,W.G.; Brinker,C.J., Eds.; Materials Research Society, Pittsburgh, 1992, 257.
50. Van Vlierberge-Torgerson, B.A.; Dulebohn, J.I.; Berglund, K.A. in *Chemical Processes of Advanced Materials*, Hench, L.L.; West, J.K., Eds.; John Wiley & Sons, Inc., 1992, 415.
51. Severin, K.G.; Ledford, J.S.; Torgerson, B.A.; Berglund, K.A. *Chem. Mater.*, in press.
52. Brinker, C.J.; Scherer, G.W. *Sol-Gel Science: The Physics and Chemistry of Sol-Gel Processing*, Academic Press, Inc., London, 1990.
53. Yoldas, B.E. *J. appl. Chem. Biotechnol.*, **1973**, 23, 803.
54. Yoldas, B.E. *Ceram. Bull.*, **1975**, 54(3), 289.
55. Pierson, H.O. *Handbook of Chemical Vapor Deposition: Principles, Technology and Applications*, Noyes Publications, Park Ridge, NJ, 1992.
56. Fix, R.M.; Gordon, R.G.; Hoffman, D.M. *Chem. Mater.*, **1990**, 2(3), 235.
57. Ghandi, S.K.; Bhat, I.B. *MRS Bull.*, Nov. **1988**, 37.
58. Besmann, T.M.; Stinton, D.P.; Lowden, R.A. *MRS Bull.*, Nov. **1988**, 45.

59. Interrante, L.V.; Sigel, G.A.; Garbauskas, M.; Hehna, C.; Slack, G.A. *Inorg. Chem.*, **1989**, 28(2), 252.
60. Ryabova, L. A.; Sasvitskaya, *J. Vac. Sci. Technol.*, **1969**, 6, 934.
61. Fischer, H.E; Larkin, D.J.; Interrante, L.V.; *MRS Bull.*, Apr. **1991**, 59.
62. *Vapor Deposition*, Powell, C.F.; Oxley, J.H.; Blocher, J.M., jr., Eds.; John Wiley & Sons, New York, 1966.
63. Gardiner, R.; Brown, D.W.; Kirlin, P.S.; Rheingold, A.L. *Chem. Mater.*, **1991**, 3, 1053.
64. Cho, C.; Hwang, D.; No, K.; Chun, J.S.; Kim, S. *J. Mat. Sci.*, **1993**, 28, 2915.
65. Chen, L.; Piazza, T.W.; Schmidt, B.E.; Kelsey, J.E.; Kaloyeros, A.E.; Hazelton, D.W.; Walker, M.S.; Luo, L.; Dye, R.C.; Maggiore, C.J.; Wilkens, E.J.; Knorr, D.B. *J. Appl. Phys.*, **1993**, 73(11), 7563.
66. Feldman, L.C.; Mayer, J.W. *Fundamentals of Surface and Thin Film Analysis*, Elsevier Science Publishing Co., Inc., New York, 1986, 225.
67. Scofield, J.H. *J. Electron Spec. Relat. Phenomena*, **1976**, 8,129.
68. Penn, D.R. *J. Electron Spec. Relat. Phenomena*, **1976**, 9, 29.
69. *Practical Surface Analysis by Auger and X-ray Photoelectron Spectroscopy*, Briggs,D.; Seah, M.P., Eds., John Wiley & Sons, Inc.Chichester, 1983, 186.
70. Hercules, D.M.; Hercules, S.H. *J. Chem. Ed.*, **1984,** 61, 483.
71. Flegler, S.L.; Heckman, J.W., jr.; Klomparens, K.L. *Scanning and Transmission Electron Microscopy an Indtroduction*, W.H. Freeman and Co., New York, 1993.

Chapter 2

Characterization of Aluminum Oxide Coatings Derived From Aluminum Valerate Thin Films

2.1. Introduction

Many early studies of aluminum based sol-gel were performed using metal nitrates or halides as sources for metal ions [1]. It is also well known that aluminum isopropoxide and sec-butoxide can be easily hydrolyzed to give various aluminum oxide-hydroxide phases, including boehmite [2-5]. Many researchers have examined the use of various inorganic acids and bases (i.e. HNO_3, HCl, H_2SO_4, HF, NH_4OH) as catalysts and peptizing agents [2-5]. Hydrolysis in a variety of organic solvents (i.e. Et_2O, benzene, alcohols) has also been studied [6,7]. The conditions chosen for these studies were largely dictated by the desire to produce monolithic, powder or colloidal forms of alumina. Significantly less attention has been given to the production of alumina thin films by the sol-gel method. There is a large literature on the chemistry involved and the structure of the gels and precursors for these syntheses [2,5,8-14]. However, there have been relatively few studies of aluminum sol-gel chemistry in systems using modified alkoxides or low hydrolysis ratios [8,25,26].

Aluminum carboxylates, or soaps, were studied during the 1950's due in large part to their use as thickening agents for greases and paints [15-24]. A number of synthetic routes to aluminum carboxylates were developed during this time. Aluminum halides and sulfates were found to produce mono and di-substituted soaps when reacted with sodium carboxylates [17,19] or acid anhydrides of organic acids [23]. The other major synthesis involved the reaction of aluminum alkoxides with acid anhydrides [20,21] or directly with the carboxylic acid [16,20-22] in an organic solvent. Throughout much of the early literature on aluminum soaps there was a debate over whether or not aluminum could form tri-soaps. Mehrotra and Pande, however, showed that the previous failures to produce the tri-substituted soaps of aluminum could be explained by the displacement of carboxylate by trace amounts of water [20]. Although many of the soaps produced in these studies were observed to be gelatinous [19], the potential for sol-gel derived thin film coatings was not investigated. Only very recently has the use of organic acids for aluminum sol-gel chemistry been given attention in the literature [25,26]. In their studies, Ayral *et al.* [25,26] investigated the chemistry of alumina powders synthesized by the controlled hydrolysis of an acetate modified aluminum alkoxide in diethyl ether.

One major use of sol-gel derived species is for the formation of thin films. Alternating layers of silica and titania have found application as coatings to produce automotive rear view mirrors since the 1950's [27]. This same technology has also been successfully used for the coating of large plate glass windows with a solar reflecting titania layer for use in modern buildings [27]. Similarly, alumina thin films have much technological importance, such as diffusion barriers for composite processing and insulating layers for electronics applications.

The present study will examine the chemistry involved in the hydrolysis and polycondensation of a valerate modified aluminum isopropoxide, for the production of aluminum oxide thin films. The structures involved in solution throughout the reaction sequence will be followed with Fourier transform infrared spectroscopy (FTIR). We will also examine the influence of dip coating and spin casting for the deposition of the films produced. The films have been characterized using FTIR, X-ray photoelectron spectroscopy (XPS) and scanning electron microscopy (SEM). Once characterized these films will be calcined, and the structure of the oxide films produced will also be determined.

2.2. Experimental

Materials. Aluminum isopropoxide 98+% and valeric acid 99+% were obtained from Aldrich Chemical Co. and used without further purification. Isopropyl alcohol (<0.01% water) was obtained from Mallinckrodt Specialty Chemicals Co. Deionized, distilled water was used for all syntheses.

Film Synthesis. The valerate films were synthesized based on a procedure developed by Berglund *et al.* [28-30] using $\overset{9}{\text{acid}}$: $\overset{1}{\text{alkoxide}}$: $\overset{1.5}{\text{water}}$ ratios of 9:1:1.5. Valeric acid was added directly to the solid alkoxide in a capped vial. After vortex stirring and 10 minutes in a sonicating bath, the caps were loosened and the solutions were heated to approximately 60°C. When most of the alkoxide had dissolved, the solution was cooled to room temperature and 3.5 mL of isopropanol was added. The reaction mixture was stirred then heated to approximately 60°C until the aluminum isopropoxide was completely dissolved. The solution was cooled to room temperature and another 3.5 mL of isopropyl alcohol was added. Finally, 46 μL of water was added and the solution was given a final stirring. Initially upon the addition of water the solution became hazy, but cleared after it was stirred. Within 10 minutes the solution became a cloudy, white color and after an hour an opaque gel was formed.

Coating Techniques. Quartz slides, which were 1-2 cm on a side and 1 mm thick were used as the substrates for XPS analysis, while 13 x 2 mm KBr windows (International Crystal, Inc.) were used as substrates for the FTIR analyses. Prior to coating the quartz plates were sonicated in a methanol bath and then rinsed with methanol. The KBr windows used were polished with aluminum oxide based abrasives and checked in the FTIR for tranparency prior to coating.

Spin casting. The solutions were spin cast onto KBr and/or quartz substrates which were placed in the center of a tabletop centrifuge. Enough solution was used to completely cover the substrate surface prior to spinning. Each sample was spun for 5 minutes.

Dip coating. Substrates were dip coated by hand. Substrates were lowered into the solution, held there for 5 seconds then withdrawn at a steady rate (~ 2 sec withdrawl time). The edge of the substrate was run along the rim of the vial to allow run off of excess solution.

Processing. The films were dried in a fume hood for at least 12 hours before analysis. Calcined films were prepared in a Lindberg tube furnace under a flow of dry air (100 cc/min, medical grade air, AGA Gas Co.) passed through an in line molecular sieve filter. After a 10 minute purge, the furnace was heated to 400°C and maintained at that temperature for 1 hour. The films were then allowed to cool to room temperature before the air flow was interrupted.

Fourier Transform Infrared Spectroscopy (FTIR). A Mattson Instruments Galaxy 3020 Fourier transform infrared spectrometer equipped with a standard DTGS detector was used to obtain infrared spectra. KBr crystals (International Crystal, Inc.) were used as substrates. Each film spectrum is an average of 16 scans at 2 cm^{-1} resolution. The reference spectrum for alumina was obtained from aluminum oxide powder (anhydrous, Fisher Scientific Co.), which was suspended in a hexane solvent and spray coated onto a KBr window.

X-Ray Photoelectron Spectroscopy (XPS). Films cast on quartz slides were analyzed with a Perkin-Elmer surface science instrument equipped with a Mg anode (1253.6 eV) operated at a power of 300 W (15 kV and 20 mA) and a model 10-360 hemispherical energy analyzer with an omnifocus small spot lens. The instrument typically operates at pressures below 1×10^{-8} Torr in the analysis chamber. Spectra were collected with a constant analyzer pass energy of 50 eV using a PC137 board interfaced to a Zeos 386SX computer. Four regions were examined for each sample: Si 2p, C 1s, Al 2p, and O 1s. Binding energies were referenced to carbon (C 1s = 284.6 eV). Empirical sensitivity factors were used to calculate atomic ratios [31]. XPS spectra were fit with 20% Lorentzian-Gaussian mix Voigt functions using a non-linear least squares curve fitting program [32].

Scanning Electron Microscopy (SEM). Samples were coated with an Emitech K-450 carbon evaporator and mounted on an aluminum stub with a low vapor pressure double sided adhesive tab (M.E. Taylor Engineering, Inc.). Samples were then analyzed at a 39 mm working distance using a JEOL JSM-35CF Scanning Electron Microscope. The micrographs shown are the secondary electron images obtained with a beam energy of 10 kV.

2.3. Results and Discussion

FTIR Spectra. *Precursors.* The FTIR spectra of aluminum isopropoxide, valeric acid and isopropanol are presented in Figure 2.1. Some of the bands of the aluminum isopropoxide spectrum (Figure 2.1a) have been assigned previously [33]. The band at 1041 cm^{-1} was attributed to the C-O stretch of the alkoxy group. The series of bands at 703, 683, 616, 573 cm^{-1} correspond closely to those observed by Barraclough [33] and Bell *et al.* [34] and have been attributed to Al-O stretches.

The assignment of the features in the valeric acid spectrum (Figure 2.1b) has been presented previously [35-37]. Methyl and methylene stretching frequencies are observed at 2962, 2935 and 2876 cm^{-1}, and are superimposed on a broad O-H absorbance centered around 3000 cm^{-1}. The band at 2671 cm^{-1} is a combination band of the C-O-H dimeric carboxylic acid stretch at 1280 cm^{-1} and the C-O-H in plane bending mode at 1414 cm^{-1}. The strong absorbance seen at 1711 cm^{-1} is due to a dimeric carboxylic carbonyl asymmetric stretch. The features centered around 1460 cm^{-1} are due to methyl and methylene vibrations. Skeletal vibrations are observed at 1380, 1109, and 750 cm^{-1}. The strong feature at 940 cm^{-1} can be assigned to an O-H out-of-plane bending mode.

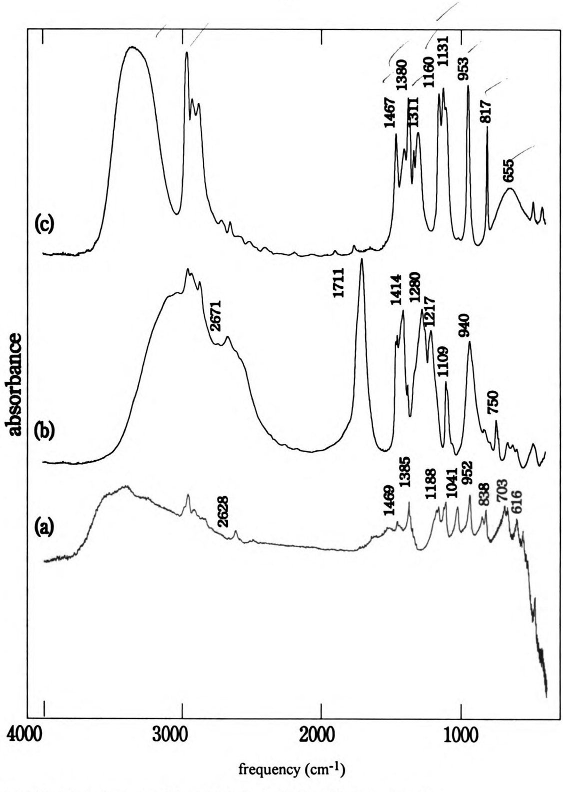

(a) Aluminum Isopropoxide (b) Valeric Acid (c) Isopropanol

Figure 2.1: FTIR Spectra for Reactants

The strongest band in the isopropanol spectrum (Figure 2.1c) is the broad O-H absorbance seen centered at 3364 cm^{-1}. Methyl and methylene stretching vibrations are observed at 2971, 2931 and 2885 cm^{-1}. Features at 1467, 1408, 1379 and 1340 cm^{-1} are assigned to the various C-H bending modes of the isopropyl group. The bands observed in the region between 1110 and 1160 cm^{-1} are associated with asymmetric C-O stretching modes of secondary alcohols. The feature at 953 cm^{-1} may be assigned to an O-H out-of-plane bending motion. The sharp feature at 817 cm^{-1} may be attributed to C-H rocking motions and C-C stretches of the isopropyl group. The features observed at 655 and 1311 cm^{-1} are out-of-plane hydroxyl bends [37].

Solutions. Figure 2.2 shows the evolution of the FTIR spectra at each step of the synthesis. Figure 2.2a shows the spectrum for a solution composed of a mixture of aluminum isopropoxide in an excess of valeric acid. A a 9:1 (acid:alkoxide) molar ratio was used to prepare this solution, however it should be noted that the spectrum was collected prior to the complete dissolution of the alkoxide. As expected, the spectrum of this solution is dominated by valeric acid features, most notably those at 1711, 1469, 1414, 1381, 1278 and 1109 cm^{-1}. Some aluminum isopropoxide features are also observed as weak bands at 1194, 1167, 1127 and 947 cm^{-1}. Intense new bands are observed at 1650 and 1585 cm^{-1}. The feature at 1650 cm^{-1} may be assigned to an asymmetric COO stretching mode associated with an ionic carboxylate group [35, 37]. The absorbance at 1585 cm^{-1} is similar to the asymmetric COO stretching frequency observed by Maksimov and Grigor'ev for the diacetate soaps of aluminum [24]. In a recent study of aluminum basic acetate, Ayral *et al.* [25, 26] assign bands at 1640 and 1580 cm^{-1} to the asymmetric COO vibrational mode for bidentate bridging and bidentate chelating acetates, respectively. The asymmetric COO bands observed at 1650 and 1585 cm^{-1} can be assigned to bridging and chelating valerate ligands, respectively. New bands at 817 and 655 cm^{-1} correspond to features observed in the isopropanol reference spectrum. Other new features are observed at 1427, 986, 916, 735, 517, and 494 cm^{-1},

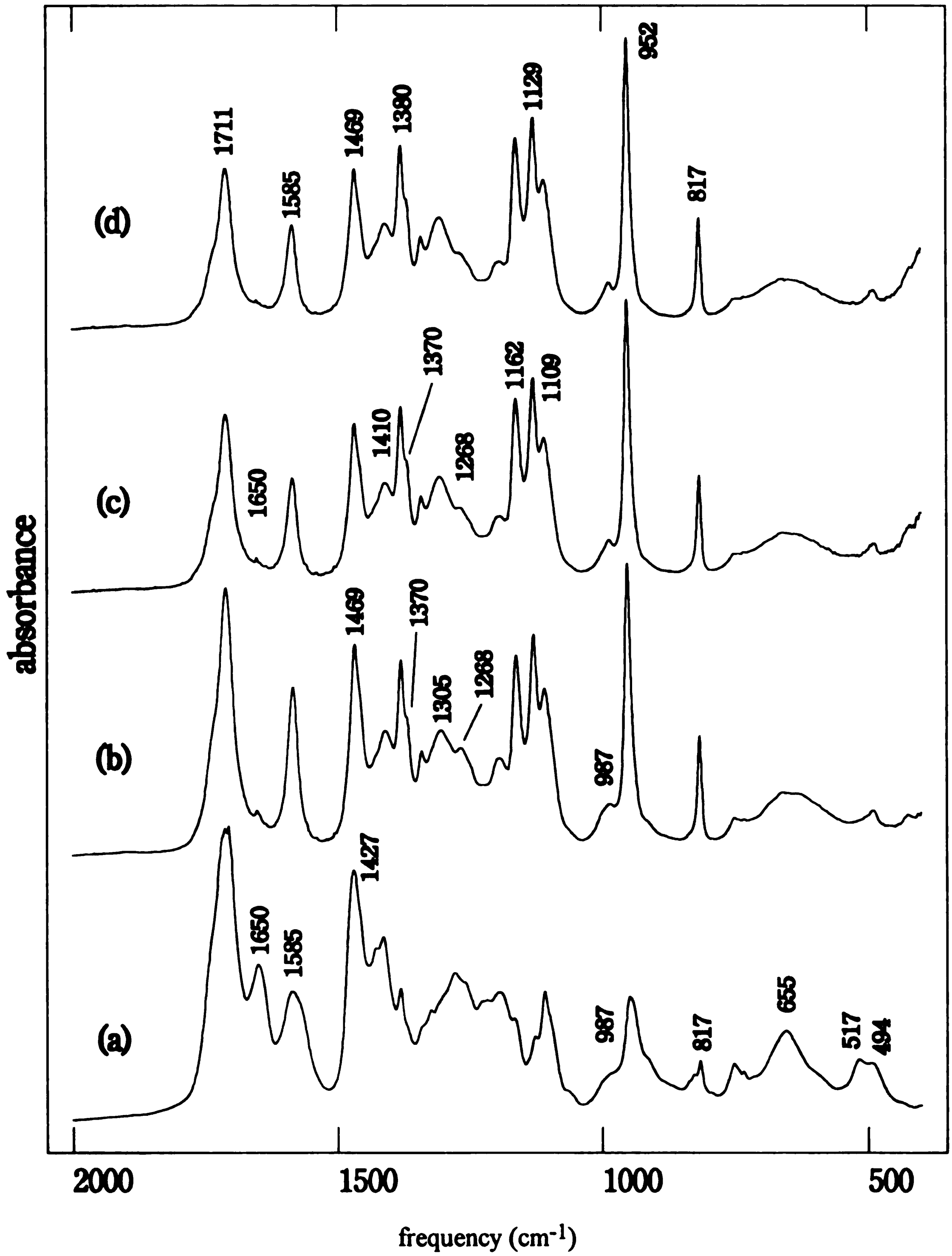

(a) Aluminum Isopropoxide and Valeric Acid (1:9)
(b) Add Isopropanol (24:1:9)
(c) Add Isopropanol (48:1:9)
(d) Add Water (1.5:48:1:9)

Figure 2.2: FTIR Spectra for Aluminum Valerate Sol-Gel Solutions

but are quite weak and exist as shoulders on other stronger bands. The shoulder at 1427 cm^{-1} is similar to that observed for COO symmetric stretches as observed in the spectra of aluminum diacetates [24]. Early IR investigation of aluminum soaps led to the assignment of a band at 985 cm^{-1} to a stretching mode for a $_2(OH)_1$ bridging OH moiety [18,22].

The assignment of the $_2(OH)_1$ band was not readily made, because it is also similar to a C-C backbone stretching frequency observed for aluminum acetates [24,38]. However, it is most likely related to the $_2(OH)_1$ vibration. If this is a band due to olation of the aluminum centers then its presence will depend on the extent of hydrolysis. However, this band is present even in the solutions containing valeric acid and aluminum isopropoxide. In this solution valerate ligands substitute for isopropoxide groups, producing isopropanol.

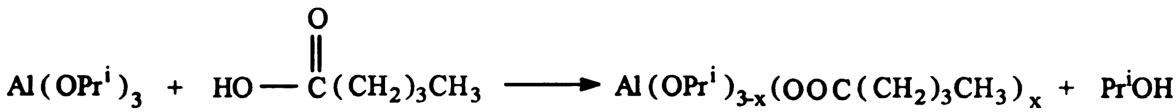

$$Al(OPr^i)_3 + HO-\overset{\overset{O}{\|}}{C}(CH_2)_3CH_3 \longrightarrow Al(OPr^i)_{3-x}(OOC(CH_2)_3CH_3)_x + Pr^iOH$$

Some hydrolysis is expected in these solutions, due to the esterification reaction between the valeric acid and the isopropanol. The change in the intensity of this band as isopropanol and water were added support this assignment. This band assignment is further supported by the calcination temperature study (Figure2.5). This band disappears from the FTIR spectrum upon heating to 200°C. However, the alkyl stretching frequencies at 2800-3000 cm^{-1}, as well as the symmetric and asymmetric C-O stretching bands for the valerate ligands are still present.

It appears that the reaction of valeric acid with the isopropoxide results in the formation of aluminum divalerates and isopropanol. Once isopropanol is released, esterification with the valeric acid can produce water, which hydrolyzes the aluminum divalerate species. The presence of the $_2(OH)_1$ feature indicates that the hydrolysis results in condensation by olation.

Figure 2.2b is the spectrum observed for a solution containing a 24 : 9 : 1 molar ratio of isopropanol : valeric acid : aluminum alkoxide. Two new bands appear in the spectrum. One is a fairly broad absorbance centered at 1305 cm^{-1} and another, overlapping band at 1268 cm^{-1}. A large increase in intensity is observed for the 1380 cm^{-1} band and also for the band at 1585 cm^{-1}, relative to the dimeric valeric acid C=O stretch at 1711 cm^{-1}. The increased intensity of the 1380 cm^{-1} band is accompanied by the formation of a shoulder around 1370 cm^{-1}. The band at 987 cm^{-1}, attributed to the bridging hydroxyl moiety, has become more resolved from the band at 952 cm^{-1}. The intensity of the asymmetric carboxylate stretch at 1650 cm^{-1} is significantly lower in this solution.

As water is produced from the esterification reaction, hydrolysis and olation continue as indicated by the change in the 987 cm^{-1} band. The increase in the band at 1585 cm^{-1} and the decrease in the 1650 cm^{-1} feature, indicates that the hydrolysis process favors the removal of bridging hydroxyl species and the formation of valerate chelates.

Figure 2.2c shows the spectrum observed for a solution containing a 48 : 9 : 1 molar ratio of isopropanol : valeric acid : aluminum alkoxide. With the increased amount of isopropanol, three significant changes in the FTIR spectra are observed. The intensity of the isopropyl skeletal vibration at 1380 cm^{-1} increases relative to the 1469 cm^{-1} band, which may be due to skeletal vibrations of the isopropanol or valeric backbones and/or asymmetric COO stretches of an aluminum valerate. The feature attributed to the presence of olated aluminum species, at 987 cm^{-1}, is sharper and the intensity of the 1650 cm^{-1} asymmetric COO stretch of the bidentate bridging valerate ligand decreases.

Figure 2.2d shows the spectrum observed for the final sol-gel solution containing 48 : 9 : 1.5 : 1 molar ratio of isopropanol : valeric acid : water : aluminum alkoxide. The features are essentially the same as those found before the addition of water.

Valerate Films. Figure 2.3 shows the FTIR spectra measured for the final sol-gel solution, as well as spin cast and dip coat films after drying in air. The spectra of the films cast by the two coating methods are nearly identical. The only significant differences between the two coating techniques is that the dip coated films have a much higher absorbance and a small difference in the intensity ratio for the 1469 and 987 cm^{-1} bands. The broad hydroxyl band observed at 3356 cm^{-1} in the precursor solution disappears upon drying, but a new hydroxyl feature appears at 3691 cm^{-1}. This sharp absorbance is characteristic of non-hydrogen bonded hydroxyl groups and is close to the frequency of the hydroxyl mode observed by Maksimov and Grigor'ev [24] for aluminum diacetate soaps (3680 cm^{-1}). The dimeric valeric acid carbonyl stretch at 1711 cm^{-1} observed in the solution spectra is reduced to a weak shoulder on the asymmetric COO stretching band at 1589 cm^{-1}. In the film spectra, the asymmetric COO stretch, which is similar to the 1591 cm^{-1} band seen in the case of diacetate soaps, is the dominant feature. A band observed at 1469 cm^{-1} corresponds to a COO symmetric stretching frequency as reported for diacetate soaps of aluminum [24,38]. The next major band is observed at 987 cm^{-1} and may be due to hydroxyl bridged aluminum moiety [24,38]. In the case of the spin cast films (Figure 2.3b), the symmetric COO stretch at 1469 cm^{-1} is more intense than the 987 cm^{-1} band. However, in the dip coated films the olated aluminum moiety stretch at 987 cm^{-1} is more intense than the 1469 cm^{-1} band. The band at approximately 759 cm^{-1} is similar to one observed for the solution spectra. The broad band centered at 655 cm^{-1} due to isopropanol is not observed, however two new bands at 671 and 580 cm^{-1} are observed. Figure 2.4 gives an expanded view of the 1500 - 900 cm^{-1} region for the as-cast films. It can be seen that the shoulder on the symmetric COO mode at 1469 cm^{-1} is composed of at least two bands. The shoulder components lie at about 1436 and 1420 cm^{-1}. The shoulder at 1420 cm^{-1} can be assigned to an additional COO symmetric stretch mode associated with the ionic valerate species [35]. This mode of vibration has also been observed in the case of aluminum acetates [24, 38]. The weak feature observed at 1378 cm^{-1} has been assigned to a C-H deformation mode of the isopropyl group. Weak bands are also observed at 1366, 1323, 1286, 1244, 1207, 1193, 1111 and 1101 cm^{-1}. The band

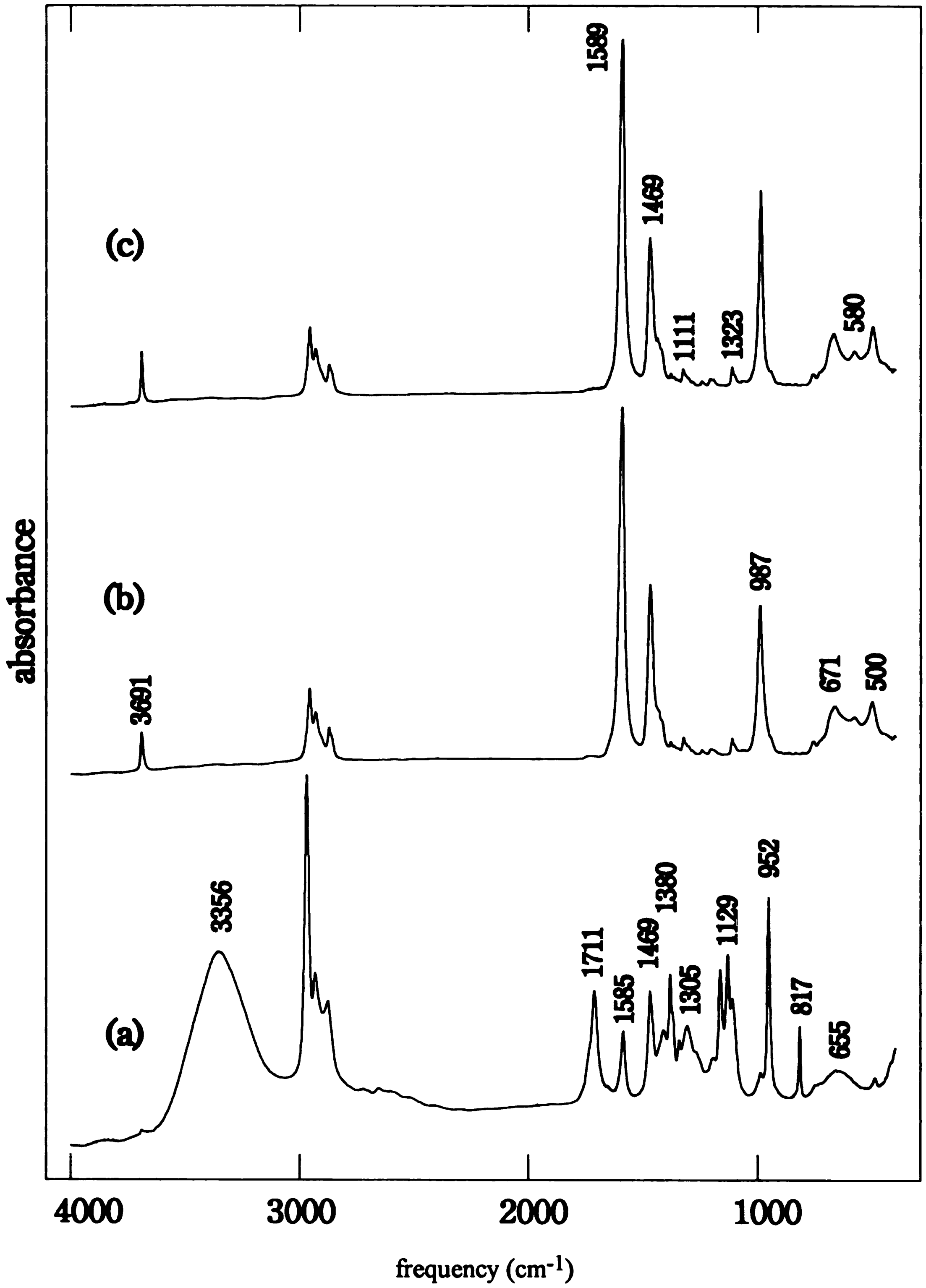

(a) Precursor solution (b) Spin cast film (c) Dip coat film

Figure 2.3: Aluminum Valerate Sol-Gel Solution and Dried Films

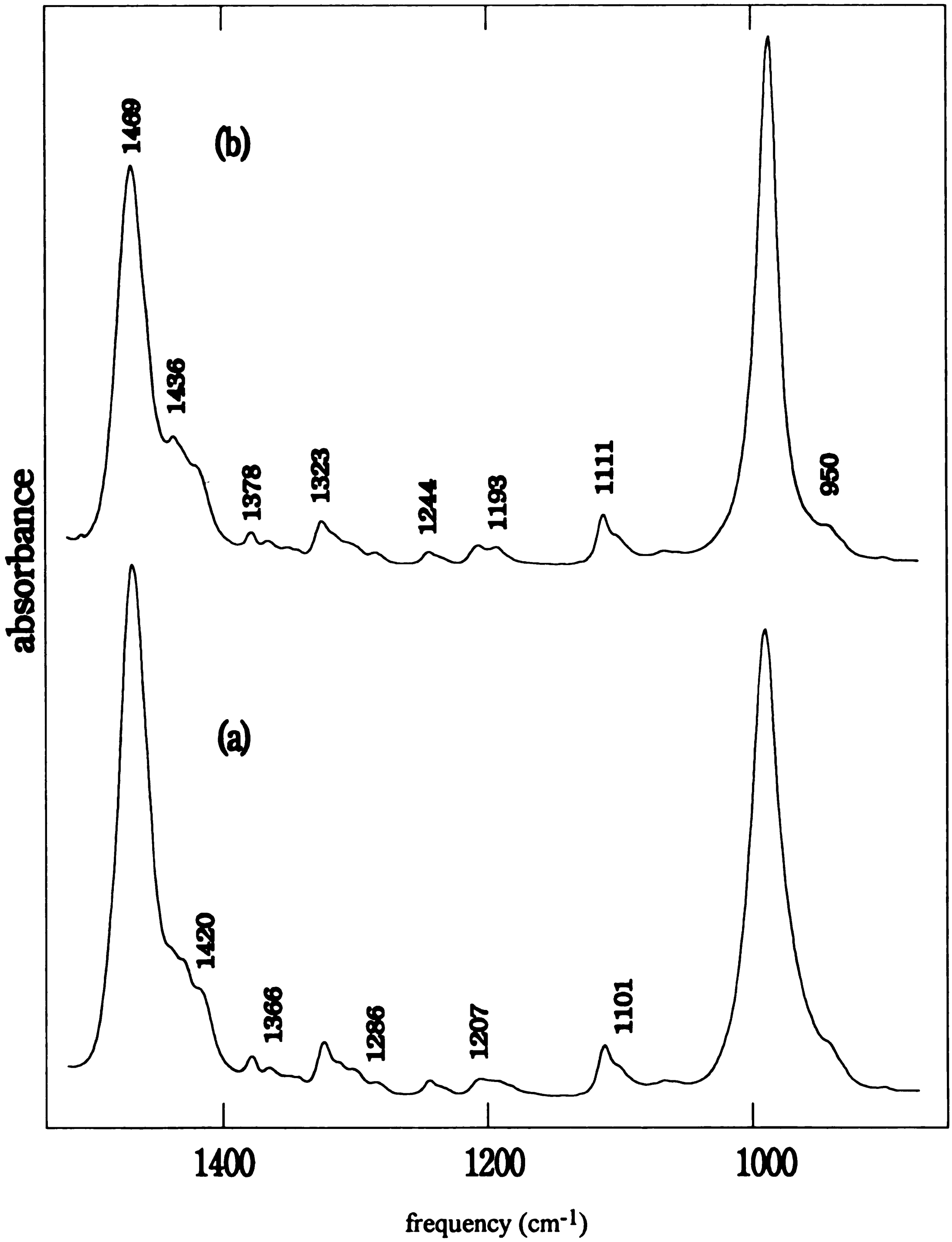

(a) Spin cast film (b) Dip coat film

Figure 2.4: FTIR Spectra: Aluminum Valerate Derived films

at 1193 cm^{-1} is consistent with COO asymmetric stretching for esters, and monomer carboxylic acids [39]. Below the 990 cm^{-1} band a shoulder at 950 cm^{-1} is observed.

Calcined Films. Figure 2.5 shows the FTIR spectra obtained for a spin cast film after calcination, as well as a spectrum for alumina powder. The first significant changes in the FTIR spectra occur at 100-200°C. In this range, the free hydroxyl stretch at 3691 cm^{-1} disappears while a broader hydroxyl stretching band centered near 3500 cm^{-1} appears. Also in this temperature range the band centered near 990 cm^{-1} is lost. From 200°C to 300°C Al-O stretching frequencies which were two distinct bands at 855 and 664 cm^{-1}, begin to coalesce giving rise to a less resolved set of bands at approximately 808 and 680 cm^{-1}. Once calcined at 400°C all of the alkyl stretching frequencies are gone, and the only bands left are the hydroxyl stretch near 3500 cm^{-1}, broad poorly resolved bands in the 1700-1400 cm^{-1} region and a single, broad Al-O stretching frequency centered at 709 cm^{-1}. The spectra of the films calcined at 400°C are similar to the alumina powder spectrum shown in Figure 2.5f. The same transitions were also observed for the dip coated films.

XPS Spectra. *Valerate Films.* The O 1s binding energy measured for both spin cast and dip coated aluminum valerate films is 531.8 eV. Two types of carbon are evident in the C 1s spectra obtained for the as cast valerate films (Figure 2.6). The C 1s component at 284.6 eV (binding energy reference) is attributed to aliphatic carbon. The second C 1s peak (288.5 eV) is due to carboxylate carbon. The Al 2p photoelectrons are observed at 74.1 eV.

The atomic ratios calculated for the as cast films are given in Table 2.1. The carboxylate carbon to aluminum ratio of 1.75 for the as cast films indicates the presence of mostly aluminum divalerate species in the film surface. The aliphatic carbon to aluminum ratio of approximately 7.7, also supports this finding, since each valerate ligand has four aliphatic carbon atoms. The oxygen to aluminum ratio for the films produced by both

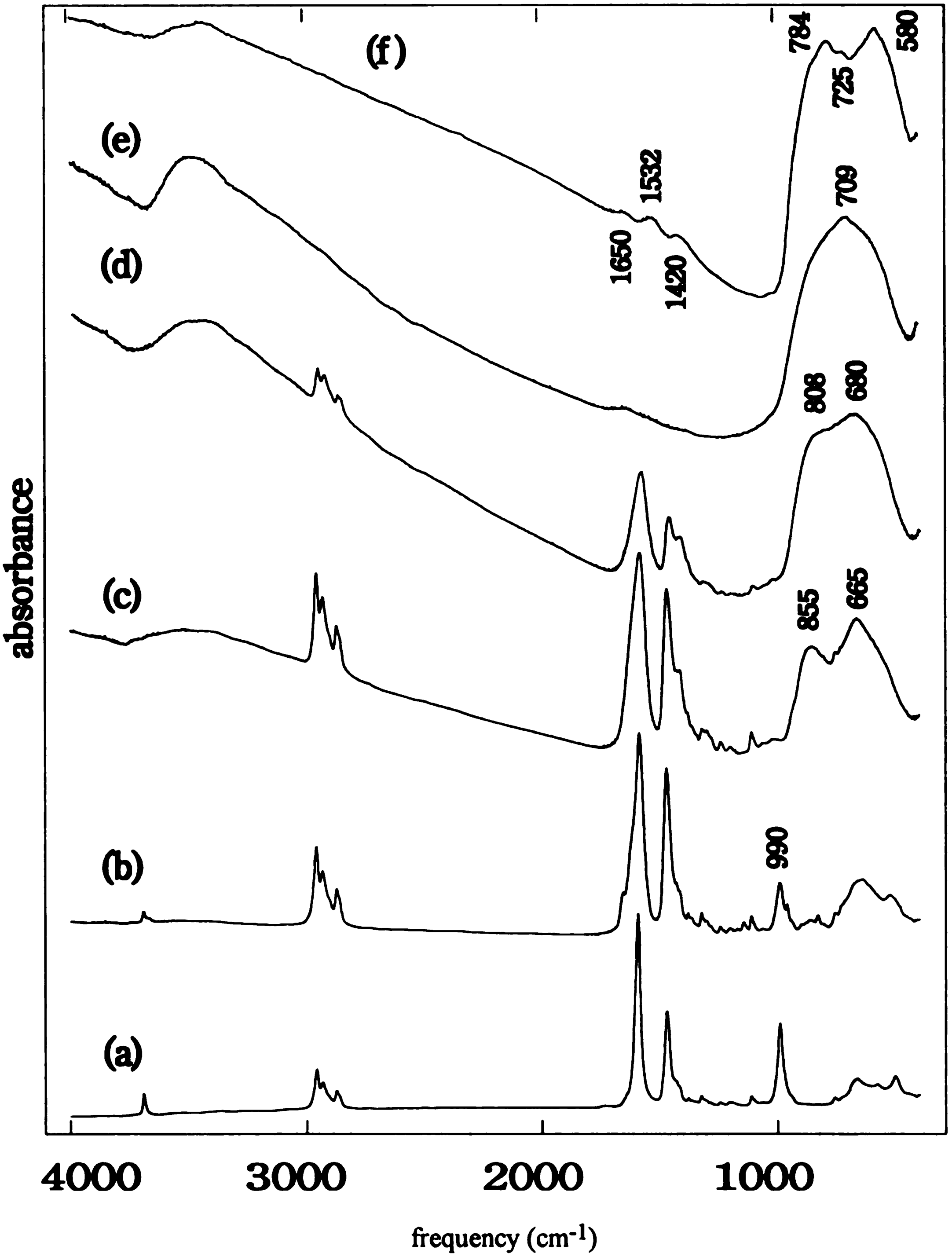

(a) Spin cast film
(b) Calcined 100°C
(c) Calcined 200°C
(d) Calcined film 300°C
(e) Calcined film 400°C
(f) Alumina standard

Figure 2.5: FTIR for Aluminum Valerate Film Calcination

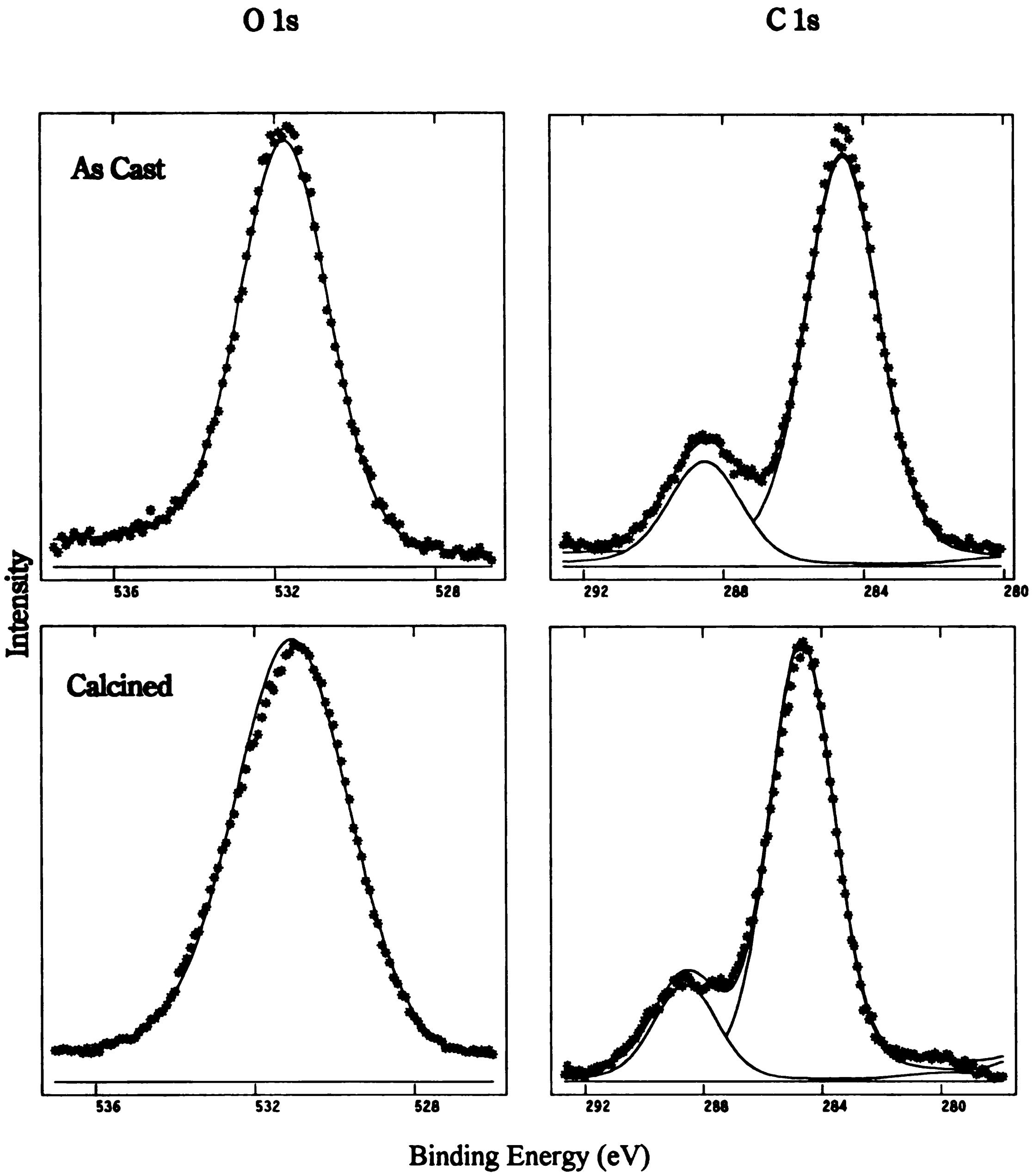

Figure 2.6: Carbon and Oxygen XPS for Films

coating methods is approximately 5. This ratio and the high oxygen 1s binding energy of 531.8 eV indicate the presence of hydroxyl species at the surface of the valerate films

Calcined Films. After calcination at 400°C, a C 1s photoelectron peak is observed at the same binding energy as the carboxylate carbon for the valerate films. The O 1s binding energy decreases to 531.1 eV for calcined films, which suggests the removal of surface hydroxyl species during the calcination process. There is no change in the Al 2p binding energy, as compared to the as cast films. No Si 2p photoelectrons were detected, indicating that the films are continuous and not cracked or agglomerated.

The oxidized carbon to aluminum ratio of 0.1 suggests that at least 95% of the valerate ligands have been removed from the surface of the films. The aliphatic carbon to aluminum ratio was found to be about 0.6 for both the spin cast and the dip coated samples. The oxygen to aluminum ratios for the calcined films were found to be 2.1.

Table 2.1 : Atomic Ratios for Aluminum Valerate Derived Films

	C (carboxyl):Al	C(aliphatic):Al	O : Al
Spin Cast / As Cast	1.75±0.15	7.6±0.3	5
Dip Coat / As Cast	1.75±0.25	7.7±1.1	5.3 ± 1.3
Spin Cast / Calcined	0.1	0.6±0.1	2.1±0.2
Dip Coat / Calcined	≤0.12	0.5±0.2	2.2 ± 0.2

SEM Results. *Valerate Films.* Figure 2.7 shows an SEM image for an as cast, dried film. The as cast dry films, both dip coated and spin cast, showed significant cracking and peeling when examined under low magnification. The surface does not look

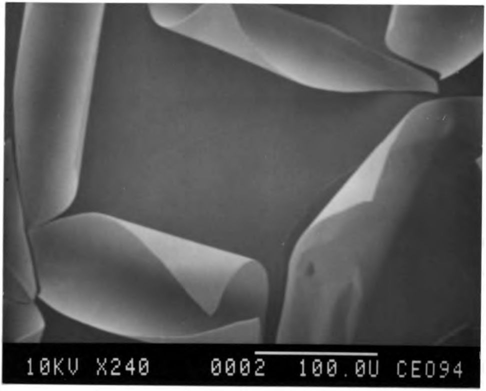

Figure 2.7: SEM of as Cast Films

lik

fil

ca

an

sm

cr

fo

ha

cr

(F

2.

sc

D

va

co

o

w

or

va

in

va

like a uniform film, but rather cracked film chips cover the surface.

Calcined Films. Figure 2.8 shows micrographs of calcined films. The calcined films look much different from the as cast films under low magnification (20-200X). The calcined films appear continuous and all of the fragmented chips seen in the as cast films are gone. Indeed, at high magnification (2,000 -10,000X) the calcined samples appeared smooth, with small specks of contaminants ≤ 5 μm (Figure 2.8). Although a few small cracks were observed at 10,000X magnification, most of the film appears to be continuous for both spin cast and dip coated samples (Figure 2.8b). The dip coated samples appear to have more variability in their morphology than the spun films. An area of patterned cracking is observed even at low magnification over half of the dip coated film sample (Figure 2.9).

2.4. Conclusions

FTIR analyses of the aluminum isopropoxide, valeric acid and isopropanol sol-gel solutions indicates that both bidentate bridging and bidentate chelating ligands are present. During hydrolysis, the bridging valerate ligands are lost preferentially to the chelating valerate species.

FTIR and XPS results for films deposited by both dip coating and spin casting are consistent with the presence of divalerate species observed for the solutions. The films obtained by dip coating are thicker and show a higher degree of olation than those which were spin cast. The higher degree of olation may be attributed to the longer drying time of a thicker film, which allows more time for the solution reactions to occur. These dried valerate films appear to be layered structures, based on the cracking and peeling observed in the SEM.

When the valerate films are calcined at 400°C, approximately 95% of the surface valerate ligands are removed, producing an aluminum oxide film. The film produced

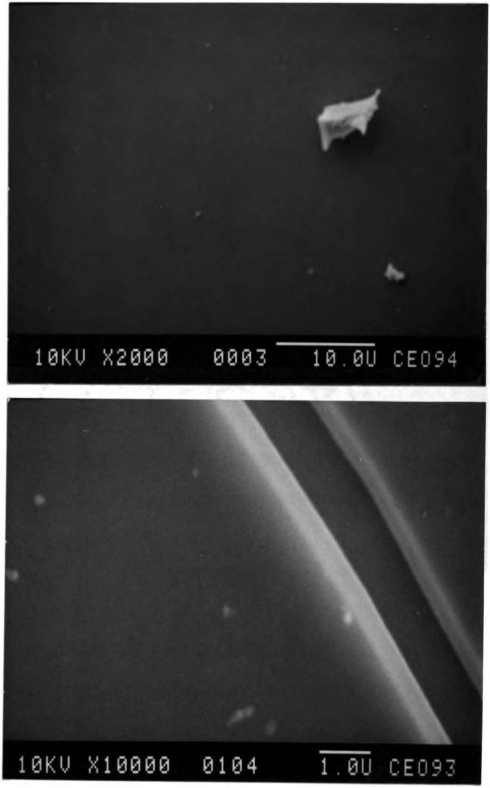

Figure 2.8: SEM of as Calcined Films

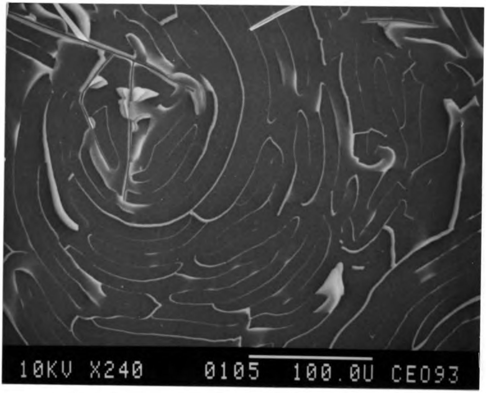

Figure 2.9: SEM of Calcined Dip Coated Film

appears to completely cover the surface. Although a few 1 μm cracks were observed in the SEM images, no photoemission from the substrate was detected.

References

1. Gitzen, W.H. *Alumina as a Ceramic Material*, The American Ceramic Society, Columbus, OH, 1970.
2. Yoldas, B.E. *J. appl. Chem. Biotechnol.*, **1973**, 23, 803.
3. Yoldas, B.E. *Ceram. Bull.*, **1975**, 54(3), 289.
4. Yoldas, B.E. *J. Mat. Sci.*, **1975**, 10, 1856.
5. Pierre, A.C.; Uhlmann, D.R. J. Am. Ceram. Soc., **1987**, 70(1), 28.
6. Harris, M.R.; Sing, K.S.W. *J. appl. Chem.*, **1957**, 7, 397.
7. Bye, G.C.; Robinson, J.G. *Kolloid Z.*, **1964**, 198,53.
8. Brinker, C.J.; Scherer, G.W. *Sol-Gel Science: The Physics and Chemistry of Sol-Gel Processing*, Academic Press, Inc., London. 1990.
9. Bye, G.C., Robinson, J.G.; Sing, K.S.W. *J. appl. Chem.*, **1967**, 17, 138.
10. Aldcroft, D.; Bye, G.C.; Robinson, J.G.; Sing, K.S.W. *J. appl. Chem.*, **1968**, 18, 301.
11. Komarneni, S.; Roy, R.; Fyfe, C.A.; Kennedy, G.J. *J. Am. Ceram. Soc.*, **1985**, 68(9), C243.
12. Olson, W.L., Bauer, L.J. in Mat. Res. Soc. Symp. Proc. 73, Brinker, C.J.; Clark, D.E.; Ulrich, D.R., Eds.; Materials Research Society, Pittsburgh, 1986, 187.
13. Nazar, L.F., Klein, L.C. *J. Am. Ceram. Soc.*, **1988**, 71(2), C85.
14. Assih, T.; Ayral, A.; Abenoza, M.;Phalippou, J. *J. Mat. Sci.*, **1988**, 23(9), 3326.
15. Gray, V.R.; Alexander, A.E. *J. Phys. Colloid Chem.*, **1949**, 53(1), 9.
16. Gray, V.R.; Alexander, A.E. *J. Phys. Colloid Chem.*, **1949**, 53(1), 23.
17. Hood, G.C.; Ihde, A.J. *J. Am. Chem. Soc.*, **1950**, 72, 2094.
18. Harple, W.W.; Wiberley, S.E.; Bauer, W.H. *Anal. Chem.*, **1952**, 24(4), 635.
19. Scott, F.A.; Goldenson, J.; Wiberley, S.E.; Bauer, W.H. *J. Phys. Chem.*, **1954**, 58, 61.
20. Mehrotra, R.C.; Pande, K.C. *J. Inorg. Nucl. Chem.*, **1956**, 2, 60.
21. Pande, K.C.; Mehrotra, R.C. *Z. anorg. allg. Chemie.*, **1956**, 286, 291.
22. Leger, A.E.; Haines, R.L.; Hubley, C.E.; Hyde, J.C., Sheffer, H. *Can. J. Chem.*, **1957**, 35, 799.
23. Maksimov, V.N.; Semenenko, K.N.; Naumova, T.N.; Novosleova, A.V. *Russ. J. Inorg. Chem.*, **1960**, 5(3), 267.
24. Maksimov, V.N.; Grigor'ev, A.I. *Russ. J. Inorg. Chem.*; **1964**, 9(4), 559.
25. Ayral, A.; Phalippou, J.; Droguet, J.C.; in Mat. Res. Soc. Symp. Proc. 121, Brinker, C.J.; Clark, D.E.; Ulrich, D.R., Eds.; Materials Research Society, Pittsburgh,1988, 239.
26. Ayral, A.; Droguet, J.C. *J. Mater. Res.*, **1989**, 4(4), 967.
27. Dislich, H. in *Sol-Gel Technology for Thin Films, Fibers, Preforms, Electronics, and Specialty Shapes*, Klein, L.C.,Ed., Noyes Publications, Park Ridge, NJ 1988, 50.
28. Gagliardi, C.D.; Dunuwila, D.; Berglund, K.A. in Mat. Res. Soc. Symp. Proc. 180, Zelinski, B.J.J.; Brinker, C.J.; Clark, D.E.; Ulrich, D.R.,Eds.; Materials Research Society, Pittsburgh, 1990, 801

29. Gagliardi, C.D.; Dunuwila, D.; Van Vlierberge-Torgerson, B.A.; Berglund, K.A. in Mat. Res. Soc. Symp. Proc. 271, Hampden-Smith, M.J.; Klemperer,W.G.; Brinker,C.J., Eds.; Materials Research Society, Pittsburgh, 1992, 257.
30. Van Vlierberge-Torgerson, B.A.; Dulebohn, J.I.; Berglund, K.A. in *Chemical Processes of Advanced Materials*, Hench, L.L.; West, J.K., Eds., John Wiley & Sons, Inc., 1992, 415.
31. Briggs, D.; Seah, M.P.; *Practical Surface Analysis, Volume 1: Auger and X-ray Photoelectron Spectroscopy*, 2nd Ed, John Wiley & Sons Ltd., Chichester, 1990. Wagner, C.D.; Davis, L.E.; Zeller, M.V.; Taylor, J.A.; Raymond, R.M.; Gale, L.H. *Surf. Interface Anal.*, **1981**, 3, 211.
32. Googly software provided by Dr. Andrew Proctor, University of Pittsburgh.
33. Barraclough, C.G.; Bradley, D.C.; Lewis, J.; Thomas, I.M. *J. Chem. Soc.*, **1961**, 2601.
34. Bell, J.V.; Heisler, J.; Tannenbaum, H.; Goldenson, J. *Anal. Chem.*, **1953**, 25(11), 1720.
35. Severin, K.G.; Ledford, J.S.; Torgerson, B.A.; Berglund, K.A. *Chem. Mater.*, in press.
36. Colthup, N.B; Daly, L.H.; Wiberley, S.E. *Introduction to Infrared and Raman Spectroscopy*, 3rd Ed., Academic Press: San Diego, 1990.
37. Silverstein, R.M.; Bassler, C.G.; Morrill, T.C. *Spectrometric Identification of Organic Compounds*, 3rd Ed., John Wiley & Sons, Inc., New York, 1974.
38. Ross, S.D.; *Inorganic Infrared and Raman Spectra*, McGraw Hill, London, 1972.
39. Smith, A.L.; *Applied Infrared spectroscopy, Fundamentals, Techniques, and Analytical Problem-solving*, John Wiley & Sons, Inc., New York, 1979.

Chapter 3

The Effect of Surface Composition on the MOCVD of Alumina From Aluminum Acetylacetonate

3.1. Introduction

The production of refractory compounds at low temperatures using chemical vapor deposition (CVD) techniques has been the focus of much attention for the last few decades [1-3]. Today CVD technology is used to produce a wide range of coatings. Currently there is much interest in the deposition of oxides, nitrides, borides and carbides. Although CVD processes generally occur at much lower temperatures than the melting point of the product, the use of metallo-organic compounds as volatile precursors has led to even further reductions in processing temperature for many compounds.

One important refractory compound is aluminum oxide. It is commonly used in optical devices, composite materials and as an electrical insulator. The classic CVD process used to obtain aluminum oxide involves the hydrolysis of aluminum halides at 1050°C [1,4].

$$2AlCl_3 + 3H_2 + 3CO_2 \xrightarrow[1\ \text{Torr}]{1050^\circ\ C} Al_2O_3 + 3CO + 6HCl$$

Organometallic compounds, however, have been shown to deposit alumina at temperatures as low as 300-500°C [5]. The deposits generally obtained at these very low temperatures are of a polycrystalline or amorphous nature. It has been shown that at temperatures above 800°C these films show γ and γ' alumina phases [6].

Much of the utility of organometallic precursors derives from the ability to design complexes which mimic both the stoichiometry and the structure of the desired product. This concept of synthetic design may also be applied to the incorporation of substituents which increase the volatility of the complex [7].

Since the discovery of high temperature 1-2-3 superconductors in 1987, the interest in MOCVD has grown due to the prospect of producing superconducting thin films via a low temperature route [8,9]. Much of this literature is focused on volatile metal β-diketonates [10-12]. The β-diketonates are chelating ligands which form ring like structures when bound to metal centers.

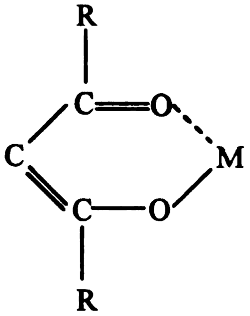

The synthesis of metal β-diketonates often involves the displacement of alkoxy ligands from a metal alkoxide in a β-diketone solvent [13]. The chelating effect of the ligand makes the metal center less sensitive to hydrolysis, and thus easier to handle than an alkoxide. Like the alkoxides, these compounds possess sufficient oxygen and high enough vapor pressures to be suitable for low temperature deposition of oxides. During the 1960's aluminum acetylacetonate was investigated as a CVD precursor. The literature reports that aluminum oxide deposits were formed at temperatures of 350-500°C [14].

Much of the research in deposition processes has focused on the effect of processing parameters, such as temperature, pressure, reactor design and carrier gas flow rate and composition [2]. Much less attention has been given to the effect of the substrate surface structure and composition on the deposition process.

In a recent review of CVD techniques, Besmann *et al.* [15] mention that the substrate surface has an effect on growth and nucleation of films, and may act as a catalyst for the deposition reaction, but no examples of such effects were discussed. Bradley [16] and Fischer *et al.* [17] mention hydroxyl groups as a catalyst for the decomposition of alkoxides. Lindstrom and Johannesson determined that the nucleation of aluminum oxide onto cemented carbide cutting tools could be enhanced by applying a titanium carbide layer prior to the deposition process [18]. Ryabova and Savitskaya have determined that the deposition temperature, growth rate and activation energy for the pyrolysis increase with the conductivity of the substrate [19]. Recently the deposition of high quality $YBa_2Cu_3O_{7-x}$ thin films onto various substrates has been investigated. Commonly the deposition of these compounds is done by using single crystal dielectric materials [20]. Chen *et al.*, however, have studied the $YBa_2Cu_3O_{7-x}$ films grown on silver substrates, using metal β-diketonate precursors [8].

The present study will examine the deposition of aluminum oxide, using aluminum acetylacetonate as the precursor. The effect of the substrate composition on this process will be examined using quartz, silicon carbide and potassium bromide as substrates. The present study will also investigate the effect of the carrier gas composition, specifically nitrogen and air, on the film deposition onto quartz substrates.

3.2. Experimental

Substrates. Reaction bonded SiC plates (Goodfellow, Co.) were polished with 45 μm and 6 μm Metadi II diamond polish (Buehler). These polished samples were sonicated in hexane and rinsed with methanol. Samples were then placed into a reactor which could be evacuated to <10 Torr. After evacuation the reactor was backfilled with a 100 ml/min hydrogen (90.5%)(AGA Gas Co., Cleveland OH) flow and the temperature was raised to 500°C for 1 hour. Samples were then placed in a 50% HF / 50% water solution for 8 hours. Samples were dried and rinsed in methanol and treated again in hydrogen. Quartz microscope slides which were cut to 1 cm x 1cm were sonicated in methanol prior to deposition. KBr windows (International Crystal, Inc.; 13 mm x 2 mm) were used without any further cleaning.

Deposition. Figure 3.1 shows the vertical reactor used for all the depositions. The carrier gas used was varied, and consisted of either: medical grade air, or nitrogen (99.99 %) (AGA Gas Co., Cleveland OH). The gas flow rate was set to 50 cc/min and regulated by mass flow controllers (Porter Instrument Co.). 0.50 g of aluminum acetylacetonate (Aldrich Chemical Co.) was used as the precursor material for production of aluminum oxide coatings. The depositor was evacuated to a pressure of 1×10^{-2} Torr, then backfilled with carrier gas. After a second evacuation and backfilling, the substrate region was heated to 400±1°C. Once the substrate reached deposition temperature, the precursor was heated to 188±1°C regulated using an Omega CN 1200 temperature controller. Once the precursor temperature was reached, the deposition was performed for 45 minutes, after which both heaters were shut off. During the deposition the samples were rotated 60° every 2 minutes.

Fourier Transform Infrared Spectroscopy (FTIR). A Mattson 3020 infrared spectrometer equipped with a standard DTGS detector was used for each measurement. KBr crystals obtained from International Crystal Inc. were used as substrate materials. Each spectrum is an average of 16 scans at 2 cm^{-1} resolution.

The reference spectrum for alumina was obtained from aluminum oxide powder (anhydrous, Fisher Scientific Co.), which was suspended in a hexane solvent and spray coated onto a KBr window.

X-ray Photoelectron Spectroscopy (XPS). Samples were analyzed with a Perkin-Elmer surface science instrument equipped with a Mg anode (1253.6 eV) operated at a power of 300 W (15 kV and 20 mA) and a model 10-360 hemispherical energy analyzer with an omnifocus small spot lens. The instrument typically operates at pressures below 1×10^{-8} Torr in the analysis chamber. Spectra were collected with a constant analyzer pass energy of 50 eV using a PC137 board interfaced to a Zeos 386SX computer. Three regions were examined for each sample: C 1s, Al 2p, and O 1s, in addition to K 2p and Br 3d (for depositions onto KBr) and Si 2p (for depositions onto quartz and silicon carbide). Binding energies were referenced to carbon (C 1s = 284.6 eV). Empirical sensitivity factors were used to calculate atomic ratios [21]. XPS spectra were fit with 20% Lorentzian-Gaussian mix Voigt functions using a non-linear least squares curve fitting program [22].

Scanning Electron Spectroscopy (SEM). The quartz and KBr samples were mounted on an aluminum stub with a low vapor pressure double sided adhesive tab (M.E. Taylor Engineering, Inc.) and coated with gold in an Emscope sputter coater for 3 minutes at 20 mA. Samples were then analyzed at a 39 mm working distance using a JEOL JSM-35CF Scanning Electron Microscope. The micrographs shown are the secondary electron images obtained with a beam energy of 10-15 kV.

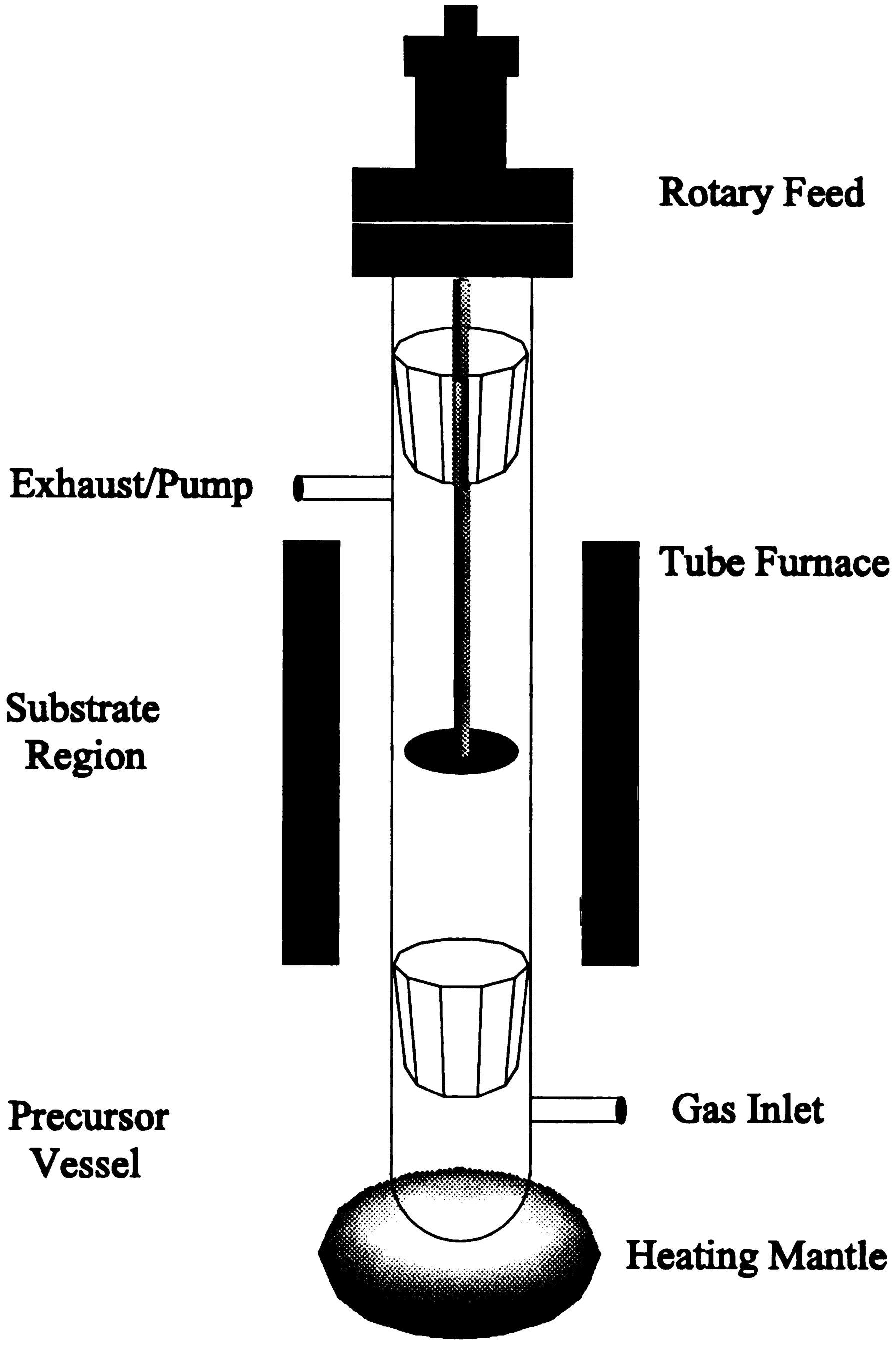

Figure 3.1 : MOCVD Depositor

3.3. Results and Discussion

FTIR Spectra. Figure 3.2 shows the FTIR spectra for the aluminum acetylacetonate precursor, film deposited at 400°C on KBr and aluminum oxide powder. The IR band assignments for aluminum acetylacetonate were published by Nakamoto *et al.* [23]. It should be noted that the spectrum collected is missing the C=O stretch at 1545 cm^{-1}, C-O stretch and C-H bend at 1466 cm^{-1}, and the out of plane bending mode at 425 cm^{-1} reported by Nakamoto *et al.* [23]. In addition, some features are observed which are not present in the reference spectrum for aluminum acetylacetonate, namely those at 1446, 1363, 1018, 951, 812, 800 and 786 cm^{-1}. All of these, except for the 800 and 786 cm^{-1} bands, are weak and appear as shoulders on the aluminum β-diketonate bands.

The spectrum measured for the film deposited at 400°C (Figure 3.2b) shows bands characteristic for the Al-O stretches, as observed for aluminum oxide powder, and a feature at 1384 cm^{-1} which can be attributed to the incomplete pyrolysis of the aluminum acetylacetonate.

XPS Spectra. The binding energy measured O 1s for depositions on SiC and KBr substrates (531.3 eV) is lower than for the depositions onto quartz (531.7-532.3 eV). This is due to the contribution of O 1s photoelectrons from the quartz substrate. The C 1s binding energy, due to oxidized carbon, measured for the deposition on quartz under nitrogen (287.1-287.4 eV) is lower than that measured for the other depositions (287.6-288.0 eV). The Al 2p binding energies measured for films deposited onto quartz (74.5-75.2 eV) are higher than those measured for the depositions onto KBr and SiC (73.8-74.2 eV).

Table 3.1 gives the XPS derived atomic ratios for the coatings deposited on quartz, silicon carbide and potassium bromide substrates, in different gas atmospheres. The oxygen to aluminum ratio was corrected to account for the O 1s photoelectrons coming from the substrate. To do this the oxygen to silicon (potassium) ratio, measured before deposition was divided by the aluminum to silicon ratio (potassium). The surface enrichment of oxygen may be due in part to the incomplete pyrolysis of aluminum acetylacetonate, or the adsorption of atmospheric water or CO_2.

Table 3.1 : Atomic Ratios for $Al(acac)_3$ MOCVD

Gas / Substrate	**O:Al**	**C:Al**	**C(ox):Al**	**Al:Si**
N_2 / SiC	1.9-5.0	≤4.9	≤0.6	18.0-37.2
N_2 / SiO_2	≤6.2	4.0-7.2	0.5-1.1	0.4-4.2
Air / SiO_2	2.4-3.5	2.6-3.8	0.3-0.9	3.2-10.6
			C(ox):K	**Al:K**
Air / KBr	1.7-2.4	0.7-1.1	0.2-0.3	5.6-6.5

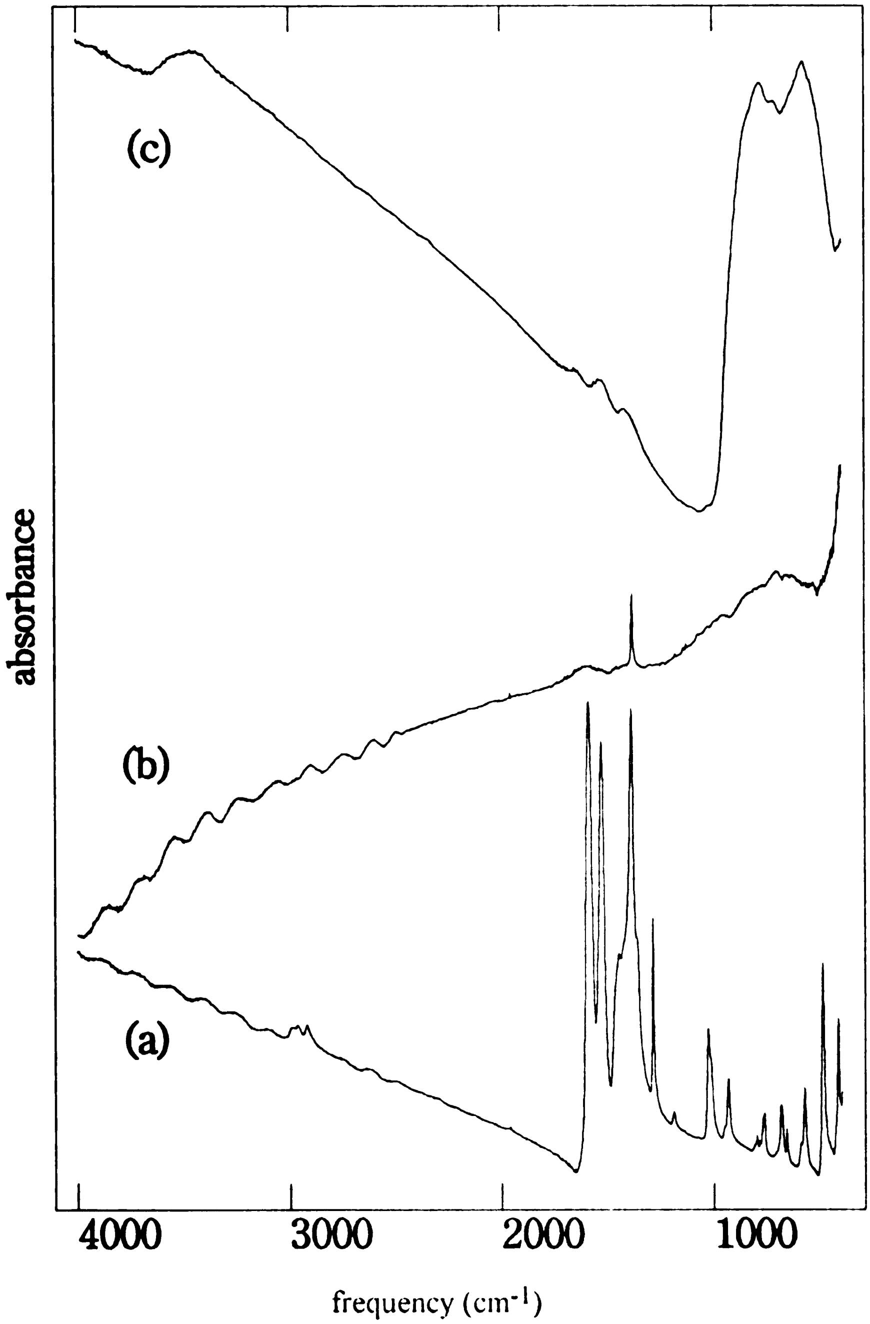

(a) Aluminum acetylacetonate (b) 400°C deposition
(c) Aluminum oxide powder

Figure 3.2: FTIR spectra for Al(acac)$_3$ deposition

The carbon to aluminum ratio for the deposition on quartz is lower when air is used as the carrier gas, compared to when nitrogen is used. This effect of the carrier gas has been seen before for depositions using β-diketonate precursors [17]. The lowest carbon to metal ratio, 0.7-1.1, was observed for the film produced on KBr in an air atmosphere.

The oxidized carbon to aluminum ratio measured for the deposition on KBr under air is found to be lower than that of the deposition onto quartz under nitrogen. These ratios indicate that 95% of the oxidized carbon of aluminum acetylacetonate is removed in the deposition on KBr in air, while for quartz under nitrogen only 80-90% removed. This finding may be due more to the carrier gas than the substrate. For the depositions on quartz under air and SiC in nitrogen the C(ox)/Al ratio indicates 85-95+% removal of oxidized carbon. This carbon may have been removed in the form of acetone, as suggested by Politycki and Hieber [24]

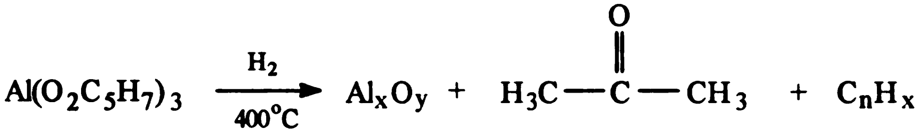

$$Al(O_2C_5H_7)_3 \xrightarrow[400^\circ C]{H_2} Al_xO_y + H_3C-\overset{\overset{O}{\|}}{C}-CH_3 + C_nH_x$$

and/or due to the breaking of the carbon-oxygen bond in the precursor.

The aluminum to silicon and aluminum to potassium ratios give an indication as to the relative amount of film growth; although it does not indicate whether the film is continuous and thin, or thick and agglomerated. The Al/Si(K) atomic ratios for the depositions on quartz and KBr were found to lie in the 0.4-10.6 range. The aluminum to silicon ratio measured for the deposition on silicon carbide in nitrogen was 18-37, possibly indicating a more efficient film growth process. At present the origin of this effect is not known. It is interesting to note, however, that the silicon carbide is a fairly covalent compound, whereas quartz and KBr are more ionic in nature. Another factor which may play a role in this effect is the sample morphology.

SEM Micrographs. The SEM micrographs of the three substrate materials used for depositions are shown in Figures 3.3 and 3.4. The silicon carbide was found to have a fairly rough surface, with pore sizes of 1-10 μm. When imaged at twice the magnification, the KBr is found to have small particulates, on the order of 0.3 μm, and grooves less than 0.1μm wide. The quartz substrate is smooth and non-porous, with stepped terrace features.

3.4. Conclusions

The FTIR and XPS results indicate that the films deposited from aluminum acetylacetonate at 400°C are structurally comparable to oxygen enriched aluminum oxide. This study has shown that the deposition of aluminum oxide from aluminum acetylacetonate produces cleaner films when air is used as a carrier gas. This study found that the cleanest films were obtained by deposition onto the ionic KBr crystal lattice under an air atmosphere. The most efficient deposition, in terms of relative amount of aluminum deposited, however, was found on the more covalent silicon carbide surface under nitrogen.

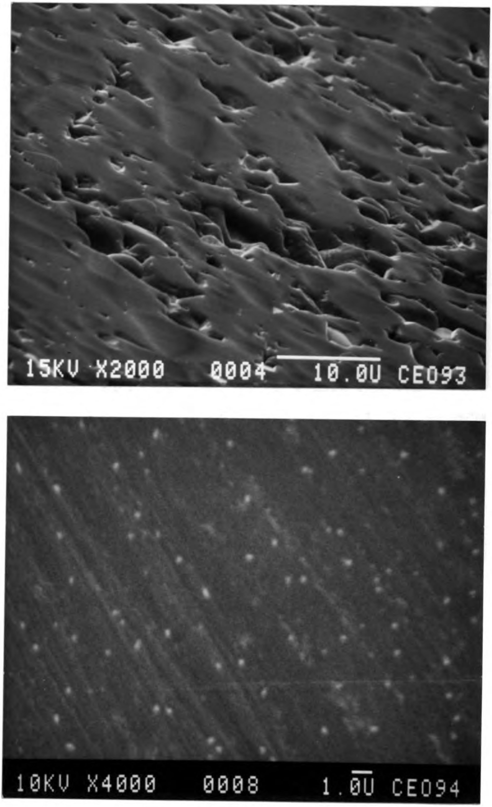

Figure 3.3: SEM Images of SiC and KBr Substrates

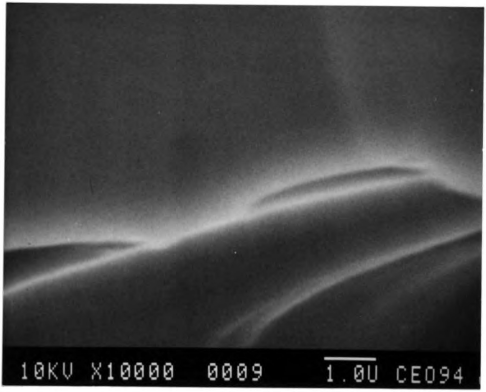

Figure 3.4: SEM Images of Quartz Substrate

References

1. Powell, C.; Oxley, J.; Blocher, J. M., Jr. *Vapor Deposition*, John Wiley & Sons, New York, 1966.
2. Pierson, H.O. *Handbook of Chemical Vapor Deposition: Principles, Technology and Applications*, Noyes Publications, Park Ridge, NJ, 1992.
3. Vossen, J.L.; Kern, W. *Thin Film Processes*, Academic Press, New York, 1978
4. Messier, D.R.; Wong, P. *J. Electrochem. Soc.*, **1971**, 118, 772.
5. Matsushita, M.;, Yoga, Y. *Electrochem. Soc. Extend. Abstr. No. 90, Spring Meeting*, **1968**, 230.
6. Aboaf, J. A.; *J. Electrochem. Soc.*, **1967**, 114, 948.
7. Interrante, L.V.; Sigel, G.A.; Garbauskas, M.; Hehna, C.; Slack, G.A. *Inorg. Chem.*, **1989**, 28(2), 252.
8. Chen, L.; Piazza, T. W.; Schmidt, B.E.; Kelsey, J. E.; Kaloteros, A. E.; Hazelton, D. W., Walker, M. S.; Luo, L.; Dye, R. C.; Maggiore, C. J.; Wilkins, D. J.; Knorr, D. B. *J. Appl. Phys.*, **1993**, 73 (11), 7563.
9. Cho, C.; Hwang, D.; No, K.; Chun, J. S.; Kim, S. *J. Mat. Sci.*, **1993**, 28, 2915.
10. Gardiner, R.; Brown, D. W.; Kirlin, P. S.; Rheingold, A. L. *Chem. Mater.*, **1991**, 3, 1053.
11. Snezhko, N.; Moroz, S.; Petchurova, N. *Mat. Sci. Eng.*, **1993**, B18, 230.
12. Buriak, J. M.; Cheatham, L. K.; Gordon, R. G.; Graham, J. J.; Barron, A. R. *Eur. J. Solid State Inorg. Chem.*, **1992**, 29, 43.
13. Mehrotra, R. C.; Bohra, R.; Gaur, D. P. *Metal β-Diketonates and Allied Derivatives*, Academic Press, London, 1978.
14. Politycki, A.; Hieber, K. in *Science and Technology of Surface Coating: a NATO Advanced Study Institute April 1972*, Ed. Chapman, B. N.; Anderson, J.C., Academic Press, London, 1974.
15. Besmann, T.M.; Stinton, D.P.; Lowden, R.A. MRS Bull., **1988**, Nov., 45
16. Bradley, D.C. *Chem. Rev.*, **1989**, 89, 1317.
17. Fischer, H.E.; Larkin, D.J.; Interrante, L.V. *MRS Bull.*, **Apr. 1991**, 59.
18. Lindstrom, J.N.; Johannesson, R.T. in *Proceedings of the Conference on Chamical Vapor Deposition, 5th International Conference 1974*, Blocher, J.M., jr.; Hintermann, H.E.; Hall, L.H., Eds.; The Electrochemical Society, 1974, 453
19. Ryabova, L. A.; Sasvitskaya, *J. Vac. Sci. Technol.*, **6**, 934, 1969
20. Chen, L; Piazza, T.W.; Schmidt, B.E.; Kelsey, J.E.; Kaloyeros, A.E.; Hazelton, D.W.; Walker, M.S.; Luo, L.; Dye, R.C.; Maggiore, C.J.; Wilkins, D.J.; Knorr, D.B. *J. Appl. Phys.*, **1993**, 73(11), 7563.
21. Briggs, D.; Seah, M.P.; *Practical Surface Analysis, Volume 1: Auger and X-ray Photoelectron Spectroscopy*, 2nd Ed, John Wiley & Sons Ltd., Chichester, 1990. Wagner, C.D.; Davis, L.E.; Zeller, M.V.; Taylor, J.A.; Raymond, R.M.; Gale, L.H. *Surf. Interface Anal.*, **1981**, 3, 211.
22. Googly software provided by Dr. Andrew Proctor, University of Pittsburgh.
23. Nakamoto, K.; McCarthy, P.J.; Ruby, A.; Martell, A.E. *J. Amer. Chem. Soc.*, **1961**, 83, 1066.

24. Politycki, A.; Hieber, K., in *Science on Technology of Surface Coatings: A NATO Advanced Study Institute April 1972*, Chapman, B.N.; Anderson, J.C., Eds.; Academic Press, London & New York, 1974.

Chapter 4

Future Work

4.1. Aluminum Sol-Gel Studies

Film Synthesis. The air dried films produced in this study appeared to be layered, since a cracked and peeling layer was observed (Figure 2.8), but the substrate was not observed using XPS. In order to produce higher quality oxide films a more complete investigation of the synthesis and processing parameters is necessary.

One of the most important factors is the rate of hydrolysis. The chemistry of alkoxides is well known, especially for the common alkoxides of aluminum such as the ethoxide, isopropoxide and sec-butoxide. In general the reactivity of the metal center in an alkoxide is found to decrease with an increase of alkyl chain length and branching. This is due to both the electron donating capabilities of the alkoxy group and also to steric hindrance. This would indicate that the hydrolysis process should proceed more slowly with the sec-butoxide. This will allow us to determine the effect of the residual alkoxide group on the aluminum sol-gel chemistry.

Another way to alter the hydrolysis chemistry of the sol-gel process is through the use of complexing agents. In the present work it was shown that valerate ligands were complexed to the aluminum centers. The use of acetic acid, such as in the work of Ayral *et al.* [1,2], could give information about the effect of the carboxylate chain length on the hydrolysis rate. Gagliardi *et al.* [3,4] have observed a reduction in the hydrolysis rate with the use of longer chain carboxylate species on titanium centers. It would also be interesting to see how the presence of a shorter carboxylate chain would effect the carbon content of the calcined films. β-diketonates are also used as a complexing agent in order to slow down the hydrolysis of transition metals [5-11]. Acetylacetone could be used in place of, or in conjunction with, the carboxylic acids in order to better control the reaction kinetics of hydrolysis and condensation.

The hydrolysis rate is expected to be directly proportional to the concentration of water present. In the present experiment water was present as a by product of the esterification reaction between valeric acid and isopropanol as well as from the addition of water in the final step of the synthesis. The synthesis could be performed without the addition of water, simply relying on the generation of water from the esterification reaction. This technique has recently been used by Laaziz *et al.* [12] for the hydrolysis of zirconium n-propoxide.

The present study used a 9:1 molar ratio of carboxylic acid to alkoxide; however, Gagliardi *et al.* [3] have shown that this ratio has dramatic effects on the properties of titanium films. In future studies, a variety of acid ratios could be investigated as a means of better controlling the film properties.

Characterization. Although the FTIR and XPS experiments of the current study have proven to be useful in the determination of structural information, they cannot describe the complete picture. For instance the FTIR data was not able to show the presence of any monodentate ligands due to overlapping bands. The FTIR and XPS techniques are also not able to determine the aluminum coordination number or the macromolecular structure of the aluminum valerate network.

Multinuclear NMR techniques have proven to be quite useful for the investigation of inorganic polymer gels. The formation of silica gels by the sol-gel route has been widely studied with ^{29}Si NMR [13-16], and the structure of these systems is well known. ^{27}Al NMR has been used to investigate the structure of alumina gels obtained by the hydrolysis of alkoxides by excess water [17-20]. These studies have shown the effectiveness of this method for probing the coordination of aluminum centers in sol-gel derived gels. Additionally, the use of ^{1}H and ^{13}C NMR might be useful in determining the more precisely the binding of the valerate ligands. Although the FTIR experiments indicate the formation of bridging and chelating valerate ligands, no quantitative information as to the relative abundance of each type of ligand exists. Further, the determination of monodentate species cannot be made with the FTIR experiments due to overlap of the their C-O stretches with other intense bands. Through NMR techniques it may be possible to determine if this type of binding is present.

Another technique which has been used to follow the sol-gel process is Raman spectroscopy. Gagliardi *et al.* [4] have examined the kinetics of the hydrolysis and condensation processes for titanium sol-gel systems using this technique. Raman spectroscopy could be used to study the time evolution of the aluminum sol-gel process.

The present work has focused on gaining molecular level structural information; however, the long range order of the polymer chains in the gels and the calcined films has not been investigated. In the case of crystalline samples, where there is very long range order, diffraction techniques such as X-ray diffraction (XRD) may be used. Although they are amorphous in nature, the gels and films obtained prior to calcination have some long range structure due to the presence metal-oxygen polymer chains. The use of small angle scattering of X-rays (SAXS) has been shown to be quite useful for probing the structure of gels [14-16]. Several theoretical models have been developed for the interpretation of SAXS data for polymer like chains [21,22]. Information related to the polymer branching and fractal dimension could be obtained from this study.

Effect of Substrate Modification on the Sol-Gel Deposition. One technique used in the synthesis of heterogeneous catalysts involves the use of grafting reactions [23]. This technique typically involves the reaction of a metal alkoxide with a hydroxyl group on a solid surface. This is similar to the alkoxide sol-gel chemistry involved in the current study. It is expected that metal alkoxide derived sol-gel films might adhere better to a hydroxylated glass surface than to a silicon carbide surface.

The surface chemistry of silicon carbide has been examined by a number of workers [24-28]. These studies have found that oxidation of the silicon carbide surface produces a surface layer of silica, whose thickness may be tailored by temperature and oxygen partial pressure. Further, the presence of silanol groups on silicon carbide has been observed with FTIR [29]. Sol-gel derived films could be deposited on clean, oxidized and hydroxylated silicon carbide substrates and their adhesion properties examined. SEM and transmission electron microscopy (TEM) investigations of the interface structure could be performed.

4.2 Aluminum Oxide MOCVD Studies

Characterization of Surface Coverage. Although some basic structural information has been obtained using XPS and FTIR, the surface coverage of the aluminum oxide films is not known. The deposited films may be very thin, but continuous or they may be thicker, but agglomerated. The lateral resolution of our XPS instrument (~3mm) and the escape depth of the photoelectrons (~ 10-100Å) limits the use of XPS in this case. If the films are very thin, (< 100Å) analysis with SEM is limited. However, the scanning Auger microprobe (SAM) has the same surface sensitivity as XPS combined with lateral resolution approaching 100 nm. Thus, the use of SAM could provide some insight into the surface coverage and nucleation of the films. Another technique which could indicate the surface coverage of the films is ion scattering spectroscopy, which has monolayer surface sensitivity.

Evaluation of the MOCVD Process. An extension of the current study is necessary in order to better examine the issue of substrate morphology on the deposition process. Prior to the SEM study of the substrate structure, it was hypothesized that an explanation for the low aluminum content observed for the silica substrates might be explained by a porous surface, which could fill with the aluminum oxide deposit but be too deep within the surface to be observed by the XPS. In fact it is the silicon carbide substrate which is the most porous surface, yet has the most aluminum relative to silicon after deposition. The deposition could be studied as a function of surface morphology simply by polishing with 1 µm and .25 µm diamond polish.

The present study found differences between the films deposited on silicon carbide and quartz. As mentioned previously, silicon carbide surfaces can be modified with layers of silica or silanol functions. An extension of the present study would be a study on the effect of surface Si-O and Si-OH groups on the deposition process. The ability to alter the deposition process by simple gas phase treatment could lead to the production of better diffusion barriers.

Presently we do not know the composition of the gas phase during the deposition process. For instance, the aluminum acetylacetonate may be partially pyrolyzed before it gets to the substrate surface. A careful study of the effects of deposition temperature and carrier gas composition may provide some insight into this.

An interesting comparison to the present study would be to use aluminum alkoxides as precursors. The deposition process could be studied as a function of the alkoxide chain length. This could provide a better understanding of the pyrolysis chemistry.

Precursor-Substrate Model Studies. Model studies of single crystal substrates might provide some insight into the chemistry involved in the CVD process. Simple gas phase treatments could be used in order to modify single crystal SiC surfaces. After the evaporation of small numbers (sub-monolayer) of precursor molecules (*eg*. $Al(acac)_3$), electron energy loss spectroscopy (EELS) could be used to probe surface vibrations. This type of information could provide details about the binding mode of precursor to the substrate. This may also lead to further information on the role of the substrate in the deposition process. Temperature programmed desorption (TPD) experiments, in conjunction with EELS could then be used to examine the changes occurring as the precursor decomposes on the surface.

4.3 Structure of Model Metal/SiC Interfaces

In order to evaluate the effectiveness of the oxide coating as a diffusion barrier, model interfaces could be prepared using Ni, Al, Nb, Fe and Ti. Interfaces could be prepared by hot pressing metal foils onto oxide coated silicon carbide substrates. After annealing at composite processing temperatures (~1000°C) these samples could be sectioned and examined with SEM, SAM and electron microprobe analysis (EPMA). The SEM could be used to evaluate the extent of reaction at both the metal/oxide and oxide/SiC interfaces. The SAM and EPMA could be used to determine structural and compositional information about the reaction zones. The progress of the reactions at the interfacial region could be studied with an *in situ* experiment. Thin (<20Å) layers of metal would be evaporated onto the coated silicon carbide samples in a UHV surface science chamber. XPS would be used to follow the reaction chemistry occurring at different temperatures.

References

1. Ayral, A.; Phalippou, J.; Droguet, J.C.; in Mat. Res. Soc. Symp. Proc. 121, Brinker, C.J.; Clark, D.E.; Ulrich, D.R., Eds.; Materials Research Society, Pittsburgh,, 1988, 239.
2. Ayral, A.; Droguet, J.C. *J. Mater. Res.*, **1989**, 4(4), 967.
3. Gagliardi, C.D.; Dunuwila, D.; Berglund, K.A. in Mat. Res. Soc. Symp. Proc. 180; Zelinski, B.J.J.; Brinker, C.J.; Clark, D.E.; Ulrich, D.R.,Eds.; Materials Research Society, Pittsburgh, 1990, 801.
4. Gagliardi, C.D.; Dunuwila, D.; Van Vlierberge-Torgerson, B.A.; Berglund, K.A. in Mat. Res. Soc. Symp. Proc. 271, Hampden-Smith, M.J.; Klemperer,W.G.; Brinker,C.J., Eds.; Materials Research Society, Pittsburgh, 1992, 257.
5. Mehrotra, R.C.; Gaur, D.P.; Bohra, R. *Metal β-diketonates and Allied Derivatives*, Academic Press, London, 1978.
6. Mehrotra, R.C.; Bohra, R. *Metal Carboxylates*, Academic Press, London, 1983.
7. Sanchez, C.; Livage, J.; Henry, M.; Babonneau, F. *J. Non-Cryst. Solids*, **1988**, 100, 65.
8. Doeuff, S.; Henry, M.; Sanchez, C.; Livage, J. *J. Non-Cryst. Solids*, **1987**, 89, 206.
9. Atik, M.; Aegerter, M.A. *J. Non-Cryst. Solids*, **1992**, 147&148, 813.
10. Chaumont, D.; Craievich, A.; Zarzycki, J. *J. Non-Cryst. Solids*, **1992**, 147&148, 127.
11. Debsikar, J.C. *J. Non-Cryst. Solids*, **1986**, 87, 343.
12. Laaziz, I.; Larbot, A.; Guizard, C.; Julbe, A.; Cot, L. in Mat. Res. Soc. Symp. Proc. 271, Hampden-Smith, M.J.; Klemperer,W.G.; Brinker,C.J., Eds.; Materials Research Society, Pittsburgh, 1992.
13. Brinker, C.J.; Clark, D.E.; Ulrich, D.R., Eds.; Mat. Res. Soc. Symp. Proc. 32, Materials Research Society, Pittsburgh, 1984.
14. Brinker, C.J.; Clark, D.E.; Ulrich, D.R., Eds.; Mat. Res. Soc. Symp. Proc. 73, Materials Research Society, Pittsburgh, 1986.
15. Brinker, C.J.; Clark, D.E.; Ulrich, D.R., Eds.; Mat. Res. Soc. Symp. Proc. 121, Materials Research Society, Pittsburgh, 1988.
16. Zelinski, B.J.J.; Brinker, C.J.; Clark, D.E.; Ulrich, D.R.,Eds.; Mat. Res. Soc. Symp. Proc. 180, Materials Research Society, Pittsburgh, 1990
17. Komarneni, S.; Roy, R.; Fyfe, C.A.; Kennedy, G.J. *J. Am. Ceram. Soc.*, **1985**, 68(9), C243.
18. Olson, W.L.; Bauer, L.J. in Mat. Res. Soc. Symp. Proc. 73, Brinker, C.J.; Clark, D.E.; Ulrich, D.R., Eds.; Materials Research Society, Pittsburgh, 1986.
19. Nazar, L.F.; Klein, L.C. *J. Am. Ceram. Soc.*, **1988**, 71(2), C85.
20. Assih, T.; Ayral, A.; Abenoza, M.; Phalippou, J. *J. Mat. Sci.*, **1988**, 23(9), 3326.
21. Feigin, L.A.; Svergun, D.I. *Structure Analysis by Small-Angle X-ray and Neutron Scattering*, Plenum Press, New York: 1987.
22. Schaefer, D.W.; Keefer, K.D. *Phys. Rev. Lett.*, **1984**, 53(14), 1383.
23. Baiker, A.; Wokaun, A. Naturwiss, **76**, 168, 1989.
24. Costello, J.A.; Tressler, R.E. J. Am. Ceram. Soc., **1986**, 69(9), 674.

25. Muehlhoff, L.; Bozack, M.J.; Choyke, W.J.; Yates, J.T., jr. *J. Appl. Phys.*, **1986**, 60(7), 2558.
26. Bellina, J.J., jr.; Ferrante, J.; Zeller, M.V. J. Vac. Sci. Technol., **1986**, A4(3), 1692.
27. Powers, J.M.; Somorjai, G.A. *Surf. Sci.*, **1991**, 244, 39.
28. Ledford, J.S.; Thelen, M.S.; Waner, M.J. Unpublished results.
29. Ramis, G.; Quintard, P.; Cauchetier, M.; Busca, G.; Lorenzelli, V. *J. Am. Ceram. Soc.*, **1989**, 72(9), 1692.